Water Resources Research

RESEARCH ARTICLE
10.1029/2022WR033597

Soil Moisture to Runoff (SM2R): A Data-Driven Model for Runoff Estimation Across Poorly Gauged Asian Water Towers Based on Soil Moisture Dynamics

Xueying Li[1,2,3], Di Long[1,2], Louise J. Slater[3], Simon Moulds[3], Muhammad Shahid[4], Pengfei Han[1,2], and Fanyu Zhao[1,2]

[1]State Key Laboratory of Hydroscience and Engineering, Department of Hydraulic Engineering, Tsinghua University, Beijing, China, [2]Key Laboratory of the Hydrosphere Sciences of the Ministry of Water Resources, Beijing, China, [3]School of Geography and the Environment, University of Oxford, Oxford, UK, [4]Faculty of Civil Engineering, University of Engineering and Technology, Lahore, Pakistan

Key Points:

- A novel model, Soil Moisture to Runoff, is proposed to simulate runoff based on soil moisture dynamics using reanalysis forcing data
- This study provides new insights into runoff estimation over poorly gauged basins without invoking any observations for calibration
- Long-term runoff over the past four decades across 20 drainage basins in seven Asian water towers is estimated

Supporting Information:

Supporting Information may be found in the online version of this article.

Correspondence to:

D. Long,
dlong@tsinghua.edu.cn

Citation:

Li, X., Long, D., Slater, L. J., Moulds, S., Shahid, M., Han, P., & Zhao, F. (2023). Soil Moisture to Runoff (SM2R): A data-driven model for runoff estimation across poorly gauged Asian water towers based on soil moisture dynamics. *Water Resources Research*, *59*, e2022WR033597. https://doi.org/10.1029/2022WR033597

Received 30 AUG 2022
Accepted 1 MAR 2023

Author Contributions:

Conceptualization: Xueying Li, Di Long
Formal analysis: Xueying Li, Di Long, Louise J. Slater, Simon Moulds, Muhammad Shahid, Pengfei Han, Fanyu Zhao
Funding acquisition: Di Long, Louise J. Slater
Methodology: Xueying Li, Di Long
Resources: Di Long, Simon Moulds, Muhammad Shahid
Software: Xueying Li
Validation: Xueying Li, Di Long, Louise J. Slater
Writing – original draft: Xueying Li
Writing – review & editing: Di Long, Louise J. Slater, Simon Moulds

Abstract Almost 2 billion people depend on freshwater provided by the Asian water towers, yet long-term runoff estimation is challenging in this high-mountain region with a harsh environment and scarce observations. Most hydrologic models rely on observed runoff for calibration, and have limited applicability in the poorly gauged Asian water towers. To overcome such limitations, here we propose a novel data-driven model, SM2R (Soil Moisture to Runoff), to simulate monthly runoff based on soil moisture dynamics using reanalysis forcing data. The SM2R model was applied and examined in 20 drainage basins across seven Asian water towers during the past four decades of 1981–2020. Without invoking any observations for calibration, the overall good performance of SM2R-derived runoff (correlation coefficient ≥0.74 and normalized root mean square error ≤0.22 compared to observed runoff at 20 gauges) suggests considerable potential for runoff simulation in poorly gauged basins. Even though the SM2R model is forced by ERA5-Land (ERA5L) reanalysis data, it largely outperforms the ERA5L-estimated runoff across the seven Asian water towers, particularly in basins with widely distributed glaciers and frozen soil. The SM2R approach is highly promising for constraining hydrologic variables from soil moisture information. Our results provide valuable insights for not only long-term runoff estimation over key Asian basins, but also understanding hydrologic processes across poorly gauged regions globally.

Plain Language Summary Long-term runoff estimation for the Asian water towers is important but challenging, which highly impacts almost 2 billion people living in downstream areas. Hydrologic models are currently the principal approach for runoff simulation. However, most hydrologic models rely on observed runoff for calibration, whose applicability is limited in the poorly gauged Asian water towers. To overcome such limitations, here we propose a novel data-driven model, SM2R (Soil Moisture to Runoff), to simulate monthly runoff based on soil moisture dynamics using reanalysis forcing data. The SM2R model was applied and examined in 20 drainage basins across seven Asian water towers during the past four decades. The overall good performance of SM2R-derived runoff suggests considerable potential for constraining hydrologic variables from soil moisture information without invoking any observations for calibration. Findings from this study are not only valuable for water availability and security for Asian water towers and downstream areas, but also for providing new insights in Prediction in Ungauged Basins globally.

1. Introduction

The Asian water towers, which include the upper regions of the Indus, Ganges, Brahmaputra, Salween, Mekong, Yangtze, and Yellow river basins, supply a large portion of both natural and anthropogenic water demands for almost 2 billion people (Yao et al., 2022). As they are relatively undisturbed by human activities, the Asian water towers serve as an important regulator in the stability of the Asian climate system but are highly sensitive to climate change (X. Li, Long, Huang, & Zhao, 2022; X. Li, Long, Scanlon, et al., 2022; Long and Li, 2022). Basin runoff is of primary interest for water availability and security in the region, and is directly linked to human water use and natural disasters (e.g., droughts and floods). Previous studies over the United States (Berghuijs et al., 2014) and European Alps (Mastrotheodoros et al., 2020) have found that as a consequence of global warming, a precipitation shift from snow toward rain leads to a decrease in observed annual runoff. However, over the

Table 1
A Summary of Previous Studies Related to Runoff Simulation Over the Asian Water Towers

Previous study	Water tower	Model	Gauge number	Time period
Immerzeel et al. (2010)	Indus, Ganges, Brahmaputra, Yangtze, Yellow	SRM	1	2000–2007
Immerzeel et al. (2013)	Indus, Ganges	Glacio-hydrological model	1	2000–2006
Lutz et al. (2014)	Indus, Ganges, Brahmaputra, Salween, Mekong	SPHY	8	1998–2007
Su et al. (2016)	Indus, Brahmaputra, Salween, Mekong, Yangtze, Yellow	VIC	6	1971–2000
Biemans et al. (2019)	Indus, Ganges, Brahmaputra	SPHY	6	1981–2010
Zhao et al. (2019)	Brahmaputra, Salween, Mekong, Yangtze, Yellow	VIC	5	1971–1990
Lutz et al. (2022)	Indus, Ganges, Brahmaputra	SPHY	6	1981–2010

Note. The time period in this table only shows historical runoff simulations in each study. SRM = Snowmelt Runoff Model; SPHY = Spatial Processes in HYdrology; VIC = Variable Infiltration Capacity.

Asian water towers, long-term runoff remains underexplored, due to the harsh environment, complex climate, and sparse in-situ observations. This hinders understanding of hydrologic processes and water resources management in both the high-mountain region and downstream areas.

Hydrologic models are currently the principal approach for runoff simulation in poorly gauged basins, but they rely heavily on the model structure and parameters (Beck et al., 2017). Observed runoff is generally essential for calibrating and validating model parameters, even though other ancillary data, such as snow cover, snow water equivalent, terrestrial water storage changes, and the drought severity index may be effective in understanding runoff processes over high-mountain water towers (Chen et al., 2017; Z. Han et al., 2021; Huang et al., 2022; Huang et al., 2020; Wu et al., 2022). Therefore, a long-standing challenge of hydrologic modeling is to extrapolate hydrologic information from gauged to ungauged/poorly gauged watersheds (Kratzert et al., 2019; Sivapalan et al., 2003). Substantial attention has been paid to runoff simulation across the Asian water towers in the past decades (e.g., Table 1), but these studies relied on hydrologic models that require observed runoff data. For example, Immerzeel et al. (2010) and Lutz et al. (2014) discussed annual runoff changes over five Asian water towers based on a snowmelt runoff model and a distributed cryospheric-hydrological model, respectively. Limited by scarce gauge observations, the reliability and applicability of these hydrologic models may not be fully examined across different Asian water towers. The risk of equifinality in hydrologic models requires caution, and may result in large discrepancy among different models during the period without observation constraint (especially for obtaining future projections). In addition, our understanding of the hydrology of the Asian water towers keeps evolving over time, as multisource data from space and ground increase, and climate and hydrological models advance. For example, Immerzeel et al. (2010) stated that the streamflow will likely decrease by the mid-21st century due to reductions in glacier meltwater in the upper Indus, Ganges, and Brahmaputra basins, whereas Lutz et al. (2014) projected an increase in runoff until at least 2050 across above basins, due to the increase in precipitation (the upper Ganges and Brahmaputra) and accelerated glacier melt (the upper Indus).

One promising approach to estimating hydrologic fluxes (e.g., precipitation, evapotranspiration (ET), and runoff) may be achieved by using soil moisture information. In recent years, approaches for flux estimation based on relationships between flux variables and soil moisture have been developed, termed SM2RAIN (Soil Moisture to Rain) because they were first applied to precipitation estimation (Brocca et al., 2013; Brocca et al., 2015). Compared to hydrologic or land surface models (LSMs), the SM2RAIN approach has more explicit physical constraints, less forcing data or prior parameters, and stronger linkage between storage and flux variables in the water balance system. Parameters in the SM2RAIN model are generally determined by multi-dimensional mathematical optimism (e.g., the gradient descent method or genetic algorithm). The objective function could potentially be constrained by using soil moisture dynamics (Akbar et al., 2019), without depending on observed runoff calibration.

Building on SM2RAIN, Akbar et al. (2019) used remote sensing-based soil moisture observations to quantify ET and drainage maps over the United States. Filippucci et al. (2020) then used in situ soil moisture and precipitation to estimate the amount of irrigation at an experimental site in Italy. However, most studies based on the SM2RAIN structure focus on the site or grid-cell scale, and assume that runoff can be neglected. For example,

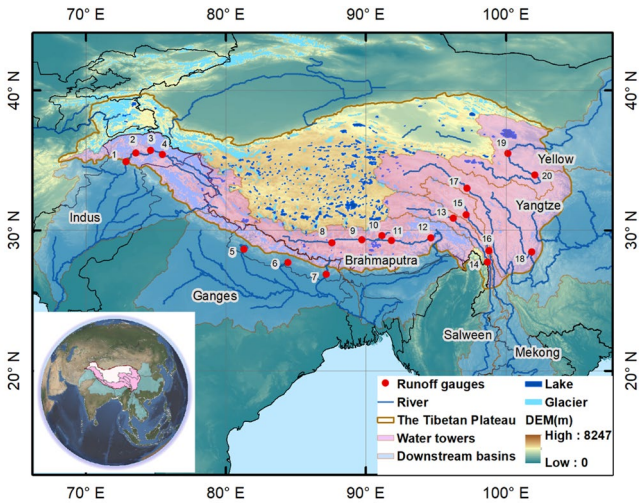

1. Besham Qila; 2. Shatial Bridge; 3. Partab Bridge Bunji; 4. Skardu Kachura; 5. Asaraghat; 6. Kali Khola; 7. Chatara; 8. Lazi; 9. Nugesha; 10. Lhasa; 11. Yangcun; 12. Nuxia; 13. Jiayuqiao; 14. Gongshan; 15. Changdu; 16. Liutongjiang; 17. Zhimenda; 18. Luning; 19. Tangnaihai; 20. Maqu

Figure 1. Location of the seven Asian water towers, runoff gauges, rivers, glaciers, and lakes. Names of runoff gauges are shown at the bottom of the figure. DEM, digital elevation model.

Brocca et al. (2013) and Akbar et al. (2019) indicated no runoff generation in the model because they assumed that all precipitation could be infiltrated into the soil. Filippucci et al. (2020) also paid no attention to surface runoff when estimating site-scale irrigation, because the optimized irrigation scheme was not expected to generate excess runoff. Although these assumptions on the neglection of runoff might be effective and reasonable at the site or grid-cell scale, they are likely to result in large non-closure of the water balance at the basin scale. In addition, current SM2RAIN studies use satellite-based soil moisture as the key input, which has inherent issues in soil moisture retrieval across the Asian water towers with widely distributed frozen soil and snow cover (Ciabatta et al., 2018). Until now, the SM2RAIN model structure has rarely been applied to basin-scale runoff estimation, particularly over the Asian water towers, and thus its potential for estimating runoff variations across this region has not yet been explored.

In this study, we proposed a novel SM2R (Soil Moisture to Runoff) model to estimate monthly runoff during the past four decades (1981–2020) across seven poorly gauged Asian water towers, including upper regions of the Indus, Ganges, Brahmaputra, Salween, Mekong, Yangtze, and Yellow basins. Developed from the SM2RAIN structure, the proposed SM2R model presents a preliminary attempt to partition precipitation into outgoing fluxes (ET, basin runoff, and drainage) over the basin scale, without invoking any runoff observations for calibration. The SM2R model is minimalistic with only seven parameters, and outgoing fluxes follow functions whose shapes are constrained by known physical processes. Apart from the basis of soil moisture dynamics, we add glacier and snow modules to improve the application of the SM2R model over regions with widely distributed glaciers and snowpack. Globally available reanalysis data are used to force the model, and parameters are constrained and optimized through the gradient descent-based multi-dimensional optimization method. Overall, the novel SM2R model suggests considerable potential for runoff analysis in poorly gauged and ungauged basins. Findings from this study are not only valuable for water availability and security for Asian water towers and downstream areas, but also for providing new insights in Prediction in Ungauged Basins (PUB) globally.

2. Study Area and Data

2.1. Study Area

The study area includes seven Asian water towers, that is, the upper regions of the Indus, Ganges, Brahmaputra, Salween, Mekong, Yangtze, and Yellow river basins that supply freshwater to China, Pakistan, India, Bangladesh, Burma, Thailand, Laos, Cambodia, and Vietnam. Here the upper regions are defined as regions within the boundary of the Tibetan Plateau, which has a mean elevation exceeding 4,000 m (Figure 1). Across the study region, both precipitation and air temperature decrease from the southeast to northwest (Hong et al., 2021; Liu, Sun, et al., 2018; Yao & Zhang, 2013). Atmospheric circulation patterns over these water towers are jointly characterized by westerlies (the Indus basin), the South Asia monsoon (the Ganges, Brahmaputra, Salween, and Mekong basins), and East Asia monsoon (the Yangtze and Yellow basins) (Li & Long, 2020; Liu et al., 2016; Yao et al., 2022). Over the southern and eastern basins that are dominated by the monsoon system, liquid precipitation (rainfall) during the monsoon period accounts for more than 60% of annual precipitation (X. Li et al., 2019; Yue et al., 2021), whereas solid precipitation (snowfall) primarily occurs in the western Indus basin.

Complex and unique hydrologic processes exist over the Asian water towers due to widespread glaciers, snowpack, permafrost and seasonally frozen soil. Glaciers are precious water resources, particularly over the Indus, Ganges, and Brahmaputra basins with concentrated glacier distributions in the Hindu Kush-Himalayas-Nyainqentanglha Mountains. Significant glacier mass loss during past decades in these mountains (Brun et al., 2017; Hugonnet et al., 2021; Zhao et al., 2022) supplies additional water input to the soil system along with precipitation (Chen et al., 2017), and largely impacts livelihoods and agriculture of densely populated downstream areas (e.g., the Indo-Gangetic Plain) (Biemans et al., 2019). Based on glacier mask data sets from the Randolph Glacier Inventory (RGI 6.0; RGI Consortium, 2017), the glacierized area accounts for ~9% (Indus), ~7% (Ganges),

Table 2
Information on the Asian Water Towers in This Study

Water tower	Location range	Elevation range (m)	Area of the water tower (km^2)	Percentage of glacier area to basin area (%)	Percentage of persistent snow cover to basin area (%)
Indus	68°–82°E 30°–37°N	779–7,528	319,695	8.5	33
Ganges	78°–88°E 27°–31°N	547–7,982	85,237	6.9	18
Brahmaputra	82°–98°E 27°–31°N	408–8,247	385,973	3.3	18
Salween	91°–99°E 26°–33°N	859–6,382	111,102	1.1	26
Mekong	94°–100°E 26°–34°N	1,403–5,983	90,802	0.3	20
Yangtze	91°–105°E 27°–36°N	781–6,317	482,063	0.3	13
Yellow	96°–104°E 32°–38°N	1,762–6,090	249,876	0.1	11

Note. Glacier areas are derived from glacier mask data sets (RGI 6.0; RGI Consortium, 2017), and percentages of persistent snow cover in each water tower are provided by Immerzeel et al. (2020).

and ∼3% (Brahmaputra) of the water tower area. In addition, snowpack stores cold-season precipitation to meet warm-season water demand in the high-mountain regions, and snowfall together with snowmelt plays a vital role in runoff generation (Liu, Wang, et al., 2018). Particularly, snowfall at high elevations (e.g., the Himalayas) often freezes in the cold seasons, resulting in a lag of several months before it melts into liquid water and causes changes in soil moisture or translates into outgoing fluxes as it gets warmer.

The frozen soil, including both permafrost and seasonally frozen ground, may impact runoff processes in headwaters of the Yangtze and Yellow basin (Shi et al., 2020; Wang et al., 2018). Warming-induced frozen soil degradation can increase soil water storage capacity and more strongly link surface and subsurface components, which further causes increases in subsurface runoff and soil evaporation. However, the relationship between frozen ground degradation and runoff generation is complicated, involving many other factors such as the vertical linkage and transfer among surface water, soil moisture, and groundwater. More information on each water tower, including the location and elevation ranges, areas, and the area percentage of glacier and persistent snow cover to the study basin is provided in Table 2.

2.2. Data

2.2.1. In Situ Runoff Observations for Model Evaluation

In-situ runoff observations from 20 gauges, which are located within and around the seven Asian water towers, are used to evaluate SM2R-simulated monthly runoff (Figure 1 and Table 3). Basin-averaged runoff depth was calculated using the total volume of basin outflow divided by the drainage area of each catchment. Daily outflow records were obtained from in-situ observations at each outlet gauge and then aggregated to monthly estimates during the 1981–2020 period. Drainage areas of these 20 basins are 16,760–205,000 km^2.

2.2.2. Reanalysis-Based Model Forcings and Soil Texture Data Sets

Volumetric soil moisture (VSM), precipitation (including snowfall and rainfall), and potential ET (PET) are the major forcings used to drive the SM2R model. Basin-averaged monthly estimates of the above variables were obtained for the period 1981–2020 from the latest land component of the fifth generation of European ReAnalysis (ERA5) data, ERA5-Land (simplified as ERA5L), provided by the European Centre for Medium Range Forecasts (ECMWF). The ERA5L estimates have the main advantage of high spatial resolution of 0.1° × 0.1° (∼10 km × 10 km), achieved through global high-resolution numerical integrations of the ECMWF land surface model driven by the downscaled meteorological forcing from the ERA5 climate reanalysis. In addition, ERA5L is reported to have large improvements in the description of the hydrological cycle, in particular with enhanced soil moisture and an overall better agreement of river discharge estimates with available observations (Munoz-Sabater et al., 2021).

Some ancillary variables of the SM2R model, including monthly air temperature, subsurface runoff, and total runoff, were also obtained from the ERA5L data sets during the 1981–2020 period. These variables were used to

Table 3
Locations, Drainage Areas, and Available Data During the 1981–2020 Period of 20 Gauges Across Seven Asian Water Towers

Water tower	Outlet gauge	Lon (°E)	Lat (°N)	Basin area (km^2)	Recording period	Data availability (months)	Data completeness (%)	Annual runoff (mm)
Indus	1. Besham Qila	72.87	34.91	192,281	1981–2018	456	100	475
	2. Shatial Bridge	73.57	35.53	183,119	1981–2007*	204	63	466
	3. Partab Bridge Bunji	74.62	35.73	171,830	1981–2018*	300	66	337
	4. Skardu Kachura	75.47	35.44	140,725	1981–2018*	444	97	315
Ganges	5. Asaraghat	81.44	28.95	20,899	1981–2010	360	100	727
	6. Kali Khola	84.55	27.83	16,760	1994–2010*	201	99	1763
	7. Chatara	87.16	26.87	54,321	1981–2010*	344	96	876
Brahmaputra	8. Lazi	87.58	29.12	47,777	2000–2010	132	100	110
	9. Nugesha	89.71	29.32	109,647	2000–2016*	181	89	167
	10. Lhasa	91.16	29.64	26,563	2001–2016*	181	94	335
	11. Yangcun	91.82	29.27	165,647	2000–2016*	169	83	221
	12. Nuxia	94.65	29.47	205,000	1981–2018	456	100	290
Salween	13. Jiayuqiao	96.24	30.87	72,844	1981–2019*	460	98	348
	14. Gongshan	98.68	27.73	105,269	1999–2016*	182	84	316
Mekong	15. Changdu	97.18	31.13	54,228	1981–2019	468	100	282
	16. Liutongjiang	98.79	28.55	77,491	2011–2017*	76	90	294
Yangtze	17. Zhimenda	97.24	33.01	139,000	1981–2017	444	100	99
	18. Luning	101.87	28.45	107,882	1981–2000	240	100	402
Yellow	19. Tangnaihai	100.15	35.50	122,749	1981–2020*	473	99	164
	20. Maqu	102.08	33.97	86,200	1981–2008	336	100	161

Note. Gauges in each water tower are listed from the west to the east, consistent with the number sequence in Figure 1. The superscript * shown in the recording period indicates that there exist missing data during the reported timespan. Annual runoff shown in the table is the mean annual basin-averaged runoff depth from observations during the recording period at each gauge.

indicate snow impacts on equivalent water input (air temperature; see Section 3.3.2), and initialize related model parameters (subsurface and total runoff; see Section 3.5). Note that model parameters initialized by the above variables are finally determined through parameter optimization (see Sections 3.5 and 3.6). All the ancillary variables were basin averaged and obtained at the monthly timescale.

Total runoff derived from ERA5L was compared with that from the SM2R model (see Section 4.3), which aims to show potential improvements in the runoff estimation mechanism driven by ERA5L inputs. The core of ERA5L for generating runoff is based on principles within the Hydrology-Tiled ECMWF Scheme for Surface Exchanges over Land (HTESSEL). The HTESSEL model considers an interception soil layer that accumulates precipitation until it is saturated, and the remaining precipitation is partitioned between surface runoff and infiltration. Subsurface water fluxes are determined by Darcy's law, used in a soil water equation solved with a four-layer discretization (Balsamo et al., 2009). In addition to the ERA5L runoff, we added comparisons with two other runoff products in Supplementary Section 1 to further evaluate the performance of SM2R-derived runoff. The supplemented runoff estimates include: (a) the China Natural Runoff Dataset (CNRD; https://doi.org/10.6084/m9.figshare.13185410) (Gou et al., 2021), and (b) the ensemble mean of 16 simulations from the second phase of the Inter-Sectoral Impact Model Intercomparison Project (ISIMIP 2b; https://data.isimip.org/) that is widely used as references for runoff analysis (Satoh et al., 2022).

Soil texture data sets were used to initialize model parameters related to drainage coefficients and the capacity of subsurface runoff (see Section 3.5). Here we used data sets from the Harmonized World Soil Database (HWSD) Version 1.2 to provided soil texture information, including available water storage capacity, aquifer specific yield, soil porosity, and weight fractions of sand and clay. The HWSD is a 30 arc-second raster database at the global scale, provided by FAO with a collaboration of IIASA, ISRIC-World Soil Information, Institute of Soil Science,

Chinese Academy of Sciences (ISSCAS), and the Joint Research Centre of the European Commission (JRC). In this study, we assumed that soil texture remained the same during the study period of 1981–2020, and used the basin-averaged estimates to represent the soil characteristics for each basin.

2.2.3. Glacier Mass Changes and Snow Cover Area

Glacier mass changes and snow cover area (SCA) are considered separately because meltwater provides additional water input for high-mountain water towers. Glacier mass changes were derived from Hugonnet et al. (2021), which were calculated by glacier elevation changes from multisource satellite archives and a glacier mask from RGI 6.0. Data sets of glacier mass changes are available globally for each individual glacier during 2000–2019 at the monthly timescale. In this study, SCA is one of indicators showing the importance of snow impacts on each basin (see Section 3.3.2), and we used mean annual persistent SCA during the 2001–2017 period processed by Immerzeel et al. (2020). This data set is based on the MODerate resolution Imaging Spectroradiometer (MODIS) snow cover product (MOD10CM) with a spatial resolution of 0.05°, and provides data for 78 water towers globally. The MODIS snow cover product has been widely used in cryosphere hydrology due to its high accuracy (Hall & Riggs, 2007; P. Han, Long, Fang, et al., 2019). Here we did not separately calculate SCA for each drainage basin of a water tower, but used the ratio of SCA to the area of the water tower as a proxy. Neither glacier mass changes nor SCA data sets covered the entire study period due to data availability. However, this could produce minor differences in runoff estimation, because (a) additional water input caused by net changes in glacier mass could be small compared with total precipitation at the large basin scale (i.e., 16,760–205,000 km^2 in this study) (see Section 4.2); (b) SCA is only an indicator to assess the importance of snow, which is not directly involved in the runoff calculation (see Section 3.3.2). The value of including the glacier and SCA data sets lies principally in completing the hydrologic cycle by including glacier and snow processes across the high-mountain Asian water towers. This approach could provide guidance for applying the SM2R model to other glacier/snow dominated basins.

3. Methodology

3.1. Framework

This study proposes a data-driven model, SM2R, to estimate long-term monthly runoff across the poorly gauged Asian water towers based on the soil water balance (Figure 2). Key points for the SM2R model include basin-scale soil water balance with the consideration of glacier and snow impacts, and mathematical functions to express relationships between outgoing fluxes and soil moisture dynamics. Using input data from reanalysis, remote sensing, and global soil texture data sets, the SM2R model estimates parameters based on the gradient descent optimization method, aiming to minimize the difference between ERA5L-derived and water balance-calculated changes in VSM. Optimized parameters in the SM2R model represent mathematical constraints among variables.

3.2. Basin-Scale Soil Water Balance

The basin-scale soil water balance reflects temporal dynamics of changes in soil moisture and water fluxes. With the soil depth z, the soil water balance equation can be expressed as Equation 1:

$$z \cdot (\Delta\theta/\Delta t) = P_{\mathrm{Eq}} - L(\theta) \tag{1}$$

where z is the soil depth (mm) that is set as one unknown depth to be optimized to ensure water balance closure (Akbar et al., 2018); θ is VSM (m^3/m^3); $\Delta\theta/\Delta t$ is the change in VSM, and the time interval Δt is 1 month; P_{Eq} is the equivalent water input for the soil system at the monthly timescale (mm/month), which results from actual rainfall, glacier mass changes, and the lag between snowfall and melt water (see Section 3.3). $L(\theta)$ is the water loss function that represents basin-averaged outgoing fluxes in the form of ET ($ET(\theta)$; mm/month), drainage ($D(\theta)$; mm/month), and runoff ($R(\theta)$; mm/month) (Equation 2). Here runoff is portioned into fast runoff, that is, surface flow ($R_{\mathrm{fast}}(\theta)$), and slow runoff, that is, subsurface flow and baseflow ($R_{\mathrm{slow}}(\theta)$) (Equation 3).

$$L(\theta) = \mathrm{ET}(\theta) + D(\theta) + R(\theta) \tag{2}$$

$$R(\theta) = R_{\mathrm{fast}}(\theta) + R_{\mathrm{slow}}(\theta) \tag{3}$$

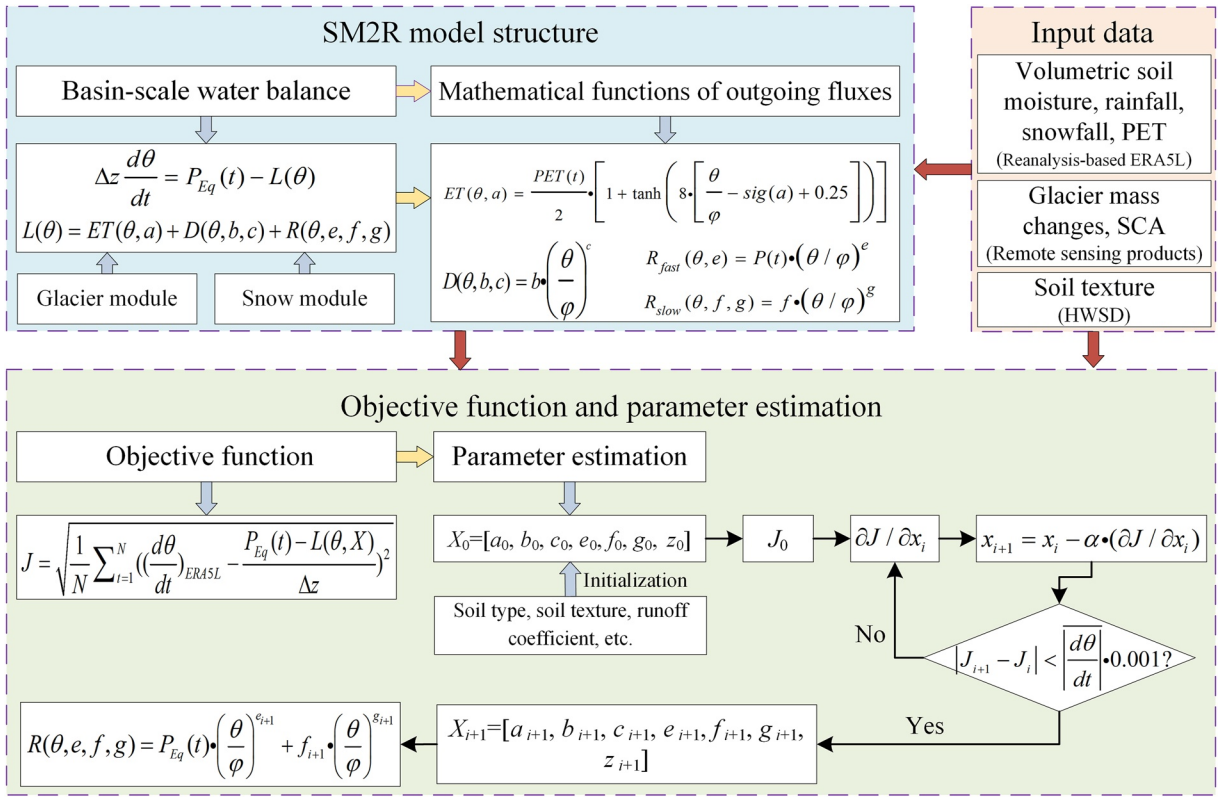

Figure 2. Flowchart of runoff estimation using the SM2R model.

3.3. Equivalent Water Input for the Soil System

Precipitation phase (i.e., rainfall and snowfall) can substantially affect cryospheric processes in high-mountain water towers and runoff generation (Z. Han et al., 2021). Thus, we partition monthly precipitation into solid (snowfall) and liquid (rainfall) phase in defining equivalent water input (P_{eq}) in Equation 1, both of which were derived from ERA5L reanalysis data.

3.3.1. Contributions of Glacier Mass Changes to Equivalent Water Input

Contributions of glacier mass changes (i.e., glacier accumulation and retreat) to soil water input can be described as the following two phases: (a) during glacier accumulation in the cold seasons, solid precipitation (snowfall) is first stored on glaciers, and then the extra water becomes available input to the soil system (Equation 4); (b) during glacier mass loss in the warm seasons, glaciers melt as liquid water, providing additional liquid water (rainfall) to recharge the soil aquifer (Equation 5).

$$\text{snowfall}_g = \begin{cases} \text{snowfall}, \text{dh}_g < 0 \\ \text{snowfall} - |\text{dh}|, \text{dh}_g \geq 0 \end{cases} \tag{4}$$

$$\text{rainfall}_g = \begin{cases} \text{rainfall} + |\text{dh}|, \text{dh}_g < 0 \\ \text{rainfall}, \text{dh}_g \geq 0 \end{cases} \tag{5}$$

In Equations 4 and 5, dh_g indicates glacier elevation change (mm/month), where positive values indicate glacier accumulation but negative ones indicate retreat; snowfall_g and rainfall_g indicate equivalent snowfall and rainfall for the soil system with the consideration of glacier mass changes, respectively; and dh indicates the change in basin-averaged water depth caused by net glacier mass change, calculated by Equation 6.

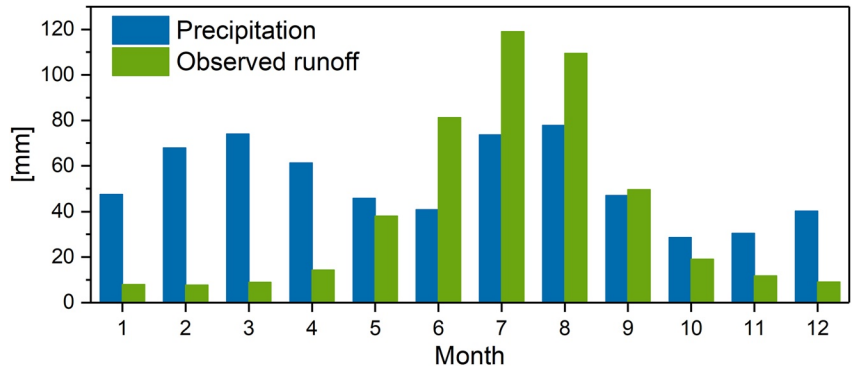

Figure 3. Mean monthly precipitation and observed runoff of a drainage basin (with the outlet gauge of Besham Qila) in the Indus water tower during 1981–2018. Precipitation data were obtained from ERA5L, and runoff was observed at the Besham Qila station.

$$\mathrm{dh} = \frac{\mathrm{dh}_g \cdot \mathrm{Area}_g \cdot \rho_g}{\mathrm{Area} \cdot \rho_w} \tag{6}$$

where Area_g indicates the area of glaciers and Area indicates the drainage area of the study basins; ρ_g is the average glacier density of 850 kg/m^3 according to Huss (2013); and ρ_w is the density of water that equals 1,000 kg/m^3.

Among the 20 drainage basins, we considered the glacier module in four basins of the Indus water tower, where glacier areas account for ∼10% of the drainage areas. For other 16 basins, the ratio of glacier area to basin area is relatively small (<5%), and thus the glacier impacts were neglected. Due to the data availability, the glacier module was applied during the 2000–2019 period. There may be minor impacts of net glacier mass changes on runoff generation across the drainage basins in this study (see Section 4.2). However, the proposed glacier module is likely to be significant in a complete hydrologic cycle, and could facilitate the application of the SM2R model to other glacier-dominated basins.

3.3.2. Impacts From High-Mountain Snowfall and Snowmelt on Equivalent Water Input

Solid precipitation (snowfall) at high elevations (e.g., the Himalayas) often freezes in the cold seasons, and there is a lag of several months before it melts into liquid water to cause changes in VSM or translates into outgoing fluxes as it gets warmer. Therefore, observed runoff may lag behind precipitation for several months and thus exhibit different peaks compared to precipitation. Taking a drainage basin in the Indus water tower as an example (Figure 3), precipitation exhibits a bimodal annual distribution, where the two peaks originate from snowfall in spring and rainfall in summer. However, there is only one peak of observed runoff which occurs in July due to both large rainfall and melt water. Water towers that store cold-season snowfall to compensate for the warm-season hydrologic cycle are defined as "snow-dominated" basins, where the cryospheric process, particularly the time lag between precipitation and runoff, plays a vital role in runoff generation.

Here we defined a Snow Index (SI) to indicate snow-dominated water towers. The SI considers the ratio of snowfall to total precipitation and the persistent snow cover throughout the year, expressed as Equation 7.

$$\mathrm{SI} = r_{\mathrm{snow/prep}} \cdot r_{\mathrm{persistent\ snow\ cover}} \tag{7}$$

where $r_{\mathrm{snow/prep}}$ means the ratio of mean annual snowfall to mean annual precipitation; $r_{\mathrm{persistent\ snow\ cover}}$ means the ratio of persistent SCA to the basin area. The proposed SI is a two-dimensional indicator for snowfall-dominated basins, considering both the amount and persistency of snow. Basins with SI > 0.16 are considered as snow-dominated water towers where the temporal lag between snowfall and runoff requires important attention. The threshold of 0.16 in SI indicates the threshold of 0.4 in both $r_{\mathrm{snow/prep}}$ and $r_{\mathrm{persistent\ snow\ cover}}$. Here the threshold of 0.4 is suggested for distinguishing basins that are highly impacted by snowfall and persistent SCA based on principles of head/tail breaks (Jiang, 2015; Jiang et al., 2013), which is a clustering scheme to divide basins into a few highly-impacted ones in the head and many less-impacted ones in the tail. The threshold of 0.4 is also widely used in related studies of distinguishing basins that are highly stressed by water resources (Huggins et al., 2022; Vorosmarty et al., 2000). In this study, only four drainage basins in the Indus water tower are identified as

snow-dominated basins. However, the snow module is significant in a complete cryospheric process, and may provide valuable insights into runoff estimation across other poorly gauged high-mountain basins globally.

For snow-dominated basins, at the monthly timescale liquid water (Rainfall_g in Equation 5) is considered to directly participate in the hydrologic cycle, that is, altering the outgoing fluxes and recharging soil moisture. However, the amount of solid water (Snowfall_g in Equation 4) that would participate in the hydrologic cycle is determined by monthly air temperature. That is, the higher the air temperature, the more snowfall_g would melt into liquid water and contribute to the hydrologic cycle. We define the melted snowfall_g as available snowfall (snowfall_a), and assume that the monthly snowfall_a is proportional to the difference between the monthly air temperature and the temperature threshold (Equation 8).

$$\text{snowfall}_a = k \cdot (T(t) - T_{\text{threshold}}) \tag{8}$$

where snowfall_a represents the available snowfall that melts into liquid water (mm/month); k is a scale factor indicating the relationship between available snowfall and the temperature difference of air temperature relative to the temperature threshold; $T(t)$ is the air temperature in each month (°C); and $T_{\text{threshold}}$ represents the temperature threshold, which is set as the mean annual air temperature minus the standard deviation of the air temperature during the study period of 1981–2020. Because at the annual timescale, the total melted available snowfall (Snowfall_a in Equation 8) should equal the actual solid water (Snowfall_g in Equation 4), the scale factor k in Equation 8 can be calculated as Equation 9:

$$k = \frac{\text{Snowfall}_a}{T(t) - T_{\text{threshold}}} = \frac{\sum \text{Snowfall}_a}{\sum (T(t) - T_{\text{threshold}})} = \frac{\sum \text{Snowfall}_g}{\sum T(t) - n \cdot T_{\text{threshold}}} \tag{9}$$

where the summation notation $\sum$ is the sum of monthly estimates for each year; and n represents the number of months that equals 12.

Overall, four drainage basins in the Indus water tower require the consideration of both glacier and snow modules in this study. The equivalent water input in these basins can be calculated as Equation 10.

$$P_{\text{Eq}} = \text{rainfall}_g + \text{snowfall}_a \tag{10}$$

The other 16 drainage basins are less impacted by snow and glacier, and the equivalent water input equals actual precipitation estimated by ERA5L.

3.4. Mathematical Functions for Estimating Outgoing Fluxes

Here we propose mathematical functions with free parameters to express relationships between soil moisture dynamics and outgoing fluxes, including ET, drainage, and runoff. The proposed functions constrain the forms (shapes) of these outgoing fluxes, guided by hydrological processes and physical principles. Unknown parameters are initialized based on soil texture and physical constraints, and finally determined by multidimensional optimization (see Sections 3.5 and 3.6).

The ET function is represented by a flexible hyperbolic tangent form that starts at zero when soil is dry and gradually increases to an asymptote when the soil is moist (Equation 11) (Akbar et al., 2019). One parameter a is employed to determine the transition of ET from water-limited to energy-limited. The parameter a is wrapped within a sigmoid function constrained from [0,1] (Equation 12), and thus, it is allowed to be unconstrained to form ET functions essentially spanning all possible transitional regimes (Akbar et al., 2019).

$$\text{ET}(\theta; a) = \frac{\text{PET}}{2}\left[1 + \tanh\left(8 \cdot \left[\frac{\theta}{\varphi} - \text{sig}(a) + 0.25\right]\right)\right] \tag{11}$$

$$\text{sig}(a) = \frac{1}{1 + e^{-a}} \tag{12}$$

where PET (mm/month) is the basin-averaged potential ET. The variable φ in Equation 11, and later used in Equations 14–16, represents the basin-averaged soil porosity. Soil porosity is calculated using the weight fractions of sand and clay (F_{sand} and F_{clay}, respectively; %) (Equation 13) (Shangguan et al., 2014).

Table 4
Drainage Coefficients for Different Soil Types

Soil type	*B*	*c*
Loamy sand	61.1	8.3
Sandy loam	25.9	11.3
Loam	13.2	15.6
Silt loam	6.8	16.2
Clay loam	2.3	17.5
Sandy clay	1.2	19.9
Clay	0.6	24.9

$$\varphi = (F_{\text{sand}} \times 0.395) + \left(F_{\text{clay}} \times 0.482\right) + \left(1 - F_{\text{sand}} - F_{\text{clay}}\right) \times 0.451 \quad (13)$$

Drainage (D) represents soil water loss vertically infiltrated into groundwater. Following Koster et al. (2018) and Jahlvand et al. (2018), we propose an exponential function (Equation 14) that captures the maximum rate of soil water loss and the reduction rate of water loss depending on the level of soil moisture saturation, controlled by the parameters b and c in Equation 14, respectively.

$$D(\theta; b, c) = b \cdot \left(\frac{\theta}{\varphi}\right)^{c} \quad (14)$$

Runoff (R) is portioned into fast and slow runoff based on the generation processes. Fast runoff (R_{fast}) is considered as a function of the equivalent water input and soil moisture, whereas slow runoff (R_{slow}) is a function of soil moisture. According to Georgakakos and Baumer (1996) and Brocca et al. (2015), fast flow is expressed as an exponential functional form (Equation 15). In addition, slow flow is also represented by an exponential form (Equation 16) to be consistent with the shape of fast flow.

$$R_{\text{fast}}(\theta; e) = P_{\text{Eq}} \cdot \left(\frac{\theta}{\varphi}\right)^{e} \quad (15)$$

$$R_{\text{slow}}(\theta; f, g) = f \cdot \left(\frac{\theta}{\varphi}\right)^{g} \quad (16)$$

The parameter e in Equation 15 controls the shape of fast flow generation, which depends on soil moisture saturation; the parameters f and g in Equation 16 capture the maximum rate and slow flow generation shape for subsurface runoff, respectively.

3.5. Parameter Initialization

Hydrologic components in the SM2R model are determined by the unknown parameter vector, $X = [a, b, c, e, f, g, z]$. Here we set the following scheme for parameter initialization based on physical constraints of different soil types. Note that parameter initialization is implemented to improve the optimization convergence efficiency and physical representativeness, but the final estimation of each parameter is determined by the optimization process (see Section 3.6).

The parameter a in Equation 11, determining the shape of the hyperbolic tangent function, can be set from unconstrained values because it is wrapped within a sigmoid function. The parameters b and c in Equation 14, determining the rate of drainage water loss, are related to soil hydraulic properties of infiltration capacity. Jahlvand et al. (2018) and Brocca et al. (2016) examined the relationship between the drainage rate and soil parameters using in situ soil observations, and provided the recommended values for b and c based on different soil types. Here we follow the mentioned two studies to initialize parameters b and c (Table 4).

The parameter e in Equation 15 represents the efficiency from precipitation to fast flow generation, and therefore, we use the basin-averaged runoff coefficient to initialize this parameter. The runoff coefficient is calculated by the ratio of multi-year average total runoff to precipitation, both of which were estimated from the ERA5L reanalysis to provide a reference.

The parameters f and g in Equation 16 are used to determine slow runoff, where f represents the capacity of slow runoff generation. We consider that f relates to soil water storage capacity and aquifer specific yield, and the initial value of f is set as Equation 17:

$$f = z' \cdot \text{AWC} \cdot \text{SY} \quad (17)$$

where AWC (mm/m) is the available soil water storage capacity derived from the HWSD (Table 5); SY is the aquifer specific yield, showing the percentage of water that can be released by soil aquifer (%); and z' is the soil

Table 5
Available Soil Water Storage Capacity for Different Soil Classes

Soil texture	Available soil water storage capacity (mm/m)
Clay (heavy)	150
Silty clay	125
Clay	100
Silty clay loam	75
Clay loam	50
Silt	15
Silt loam	0

depth for subsurface runoff generation, which is set as 100 cm according to the reference depth for estimating AWC from the HWSD. For soils below 100 cm, we suppose that vertical drainage instead of subsurface flow is the major process of soil water loss.

The parameter g represents the shape of slow runoff, which is initialized by the ratio of multi-year average subsurface runoff to multi-year average total runoff, both of which are derived from the ERA5L reanalysis to provide a reference. The last parameter z indicates the soil depth to meet the water balance in Equation 1. Because the major input data are derived from ERA5L, we use the soil depth in ERA5L reanalysis (i.e., 2,890 mm) to initialize the parameter z.

3.6. Objective Function and Parameter Estimation

The objective function to be minimized is set as the root mean square error between ERA5L-derived and water balance-calculated changes in VSM (Equation 18):

$$J = \sqrt{\frac{1}{n}\sum_{t=1}^{n}\left(\left(\frac{d\theta}{dt}\right)_{ERA5L} - \left(\frac{P_{\mathrm{Eq}} - L(\theta, X)}{z}\right)\right)^2} \tag{18}$$

Here the optimization object is changes in VSM, that is, $\frac{d\theta}{dt}$. We set the optimization threshold (ε) as the 1‰ of the magnitude of the optimization object (Equation 19). The optimization threshold indicates the acceptable criterion to terminate the iteration. It means that if the difference between two iterative optimizations is less than this threshold (Equation 20), the improvement of the objective function is very limited and thus the optimization process can be completed. The threshold in this study can be considered as a reference for the balance between optimization performance and iteration times, and one can set other thresholds according to the accuracy requirements, for example, a smaller threshold with more iteration times.

$$\varepsilon = 0.001 \cdot \overline{\left|\frac{d\theta}{dt}\right|} \tag{19}$$

$$|J_i - J_{i-1}| < \varepsilon \tag{20}$$

The optimization algorithm is based on the gradient descent method, which is widely used in data-driven approaches (e.g., the back-propagation neural network). For each case, the optimization and estimation steps are as follows.

1. Starting with an initial guess of each parameter $X_0 = [a_0, b_0, c_0, e_0, f_0, g_0, z_0]$.
2. Forward calculating Equation 18 to obtain an initial value of the optimization function (J_0). VSM (θ) and equivalent water input (P_{Eq}) are known here.
3. Calculating the gradient of the optimization function in Equation 18, that is, $\frac{\partial J}{\partial x_i}$.
4. Applying a gradient descent update to X_0 for iteration: $x_{i+1} = x_i - \alpha \cdot \frac{\partial J}{\partial x_i}$. Here α represents the degree of optimization accuracy, which is generally set in the range of [1, 10] in the optimization iteration. In this study, we set α as 5 to calculate the update.
5. Calculating the iterated value of the objective function (J_{i+1}) based on the updated parameters in step 4.
6. Repeating steps 3–5 until the optimization function meets the termination criterion (Equation 20).
7. Reporting the optimum parameter vector $X_{i+1} = [a_{i+1}, b_{i+1}, c_{i+1}, e_{i+1}, f_{i+1}, g_{i+1}, z_{i+1}]$
8. Estimating the monthly runoff using the optimum parameters in the step 7.

3.7. Evaluation Indices and Anomaly Calculation

We chose five indices to comprehensively evaluate the performance of estimated runoff, including the Nash-Sutcliffe efficiency (NSE), logarithmic Nash-Sutcliffe efficiency coefficient (logNSE), Pearson correlation coefficient (CC), normalized root mean square error (NRMSE), and Kling-Gupta efficiency (KGE). NSE and

logNSE are normalized statistics determining the relative magnitude of residual variance (noise) relative to the measured data variance (information) (Nash & Sutcliffe, 1970), where NSE is mostly impacted by high flow but logNSE is mostly impacted by low flow. CC is used to measure the sample cross correlation between the simulated and observed values. NRMSE measures the fitness of the predictive model, and is termed as RMSE divided by the difference between the maximum and minimum of the observed values. KGE is a comprehensive indicator including correlation, ratio of means, and ratio of dispersion of the two paired data sets (Gupta et al., 2009; Kling et al., 2012). Specifically, these indices are calculated as follows:

$$\mathrm{NSE} = 1 - \frac{\sum (Q_{\mathrm{sim}} - Q_{\mathrm{obs}})^2}{\sum \left(Q_{\mathrm{obs}} - \overline{Q_{\mathrm{obs}}}\right)^2} \tag{21}$$

$$\mathrm{logNSE} = 1 - \frac{\sum (\log(Q_{\mathrm{sim}}) - \log(Q_{\mathrm{obs}}))^2}{\sum \left(\log(Q_{\mathrm{obs}}) - \log(\overline{Q_{\mathrm{obs}}})\right)^2} \tag{22}$$

$$\mathrm{CC} = \frac{\sum \left(Q_{\mathrm{sim}} - \overline{Q_{\mathrm{sim}}}\right)\left(Q_{\mathrm{obs}} - \overline{Q_{\mathrm{obs}}}\right)}{\sqrt{\sum \left(Q_{\mathrm{sim}} - \overline{Q_{\mathrm{sim}}}\right)^2} \sqrt{\sum \left(Q_{\mathrm{obs}} - \overline{Q_{\mathrm{obs}}}\right)^2}} \tag{23}$$

$$\mathrm{NRMSE} = \frac{\mathrm{RMSE}}{\max(Q_{\mathrm{obs}}) - \min(Q_{\mathrm{obs}})} \tag{24}$$

$$\mathrm{KGE} = 1 - \sqrt{(\mathrm{CC} - 1)^2 + \left(\frac{\overline{Q_{\mathrm{sim}}}}{\overline{Q_{\mathrm{obs}}}} - 1\right)^2 + \left(\frac{\mathrm{std}(Q_{\mathrm{sim}})}{\mathrm{std}(Q_{\mathrm{obs}})} - 1\right)^2} \tag{25}$$

In Equations 21–25, Q_{sim} and Q_{obs} represent the SM2R-simulated and observed runoff, respectively; an overbar denotes mean, and std represents standard deviation. Except NRMSE that has the perfect value of 0, other indices show the best performance indicated by a value of 1.

To evaluate the model performance by simulating the anomaly at both the annual and monthly timescales, we first calculated the climatological normal that is defined as the monthly average during January 1981 to December 2010. The monthly anomaly is the difference of monthly estimates relative to the climatological normal. For each year during the study period of 1981–2020, the annual anomaly is aggregated from the monthly anomaly. A positive runoff anomaly means a higher flow than the baseline, whereas a negative runoff anomaly indicates a lower flow than the long-term average.

4. Results

4.1. Performance Evaluation of SM2R-Simulated Runoff Over the Past Four Decades

Monthly runoff during the period 1981–2020 is simulated by SM2R and evaluated against observations at 20 gauges in seven Asian water towers (Table 6). In general, SM2R simulations are highly correlated with runoff observations, and the variance of simulation error is pretty low (CC $\geq$ 0.74 and NRMSE $\leq$ 0.22 at all gauges). Good performance of three comprehensive indices (i.e., NSE, logNSE, and KGE) is found at most gauges (16 gauges showing NSE > 0.56, logNSE > 0.43, and KGE > 0.46). This indicates that the SM2R model successfully captures runoff variations during the past four decades, that is, the general good simulation in both high and low flow, and the overall consistency with in-situ runoff in correlation, bias, and standard variation. Because the model performance is considered reliable with CC > 0.77 and NSE > 0.5 (Santhi et al., 2001), the SM2R model shows considerable potential for estimating long-term runoff in poorly gauged basins without relying on any observed data for calibration.

Here we further analyze the performance of the SM2R model among seven Asian water towers that are dominated by different climate and geographic features (Figure 4). SM2R-derived runoff shows a high degree of accuracy in the Indus basin that has the largest distribution of glacier and seasonal snow cover among all

Table 6
Specific Values of NSE, logNSE, CC, NRMSE, and KGE for Evaluating SM2R-Derived Runoff Based on Observations From 20 Gauges

Water tower	Gauge	Observations (months)	CC	NRMSE	KGE	NSE	logNSE
Indus	Besham Qila	456	0.94	0.10	0.69	0.82	0.65
	Shatial Bridge	204	0.94	0.10	0.73	0.85	0.77
	Partab Bridge Bunji	300	0.95	0.13	0.61	0.77	0.48
	Skardu Kachura	444	0.94	0.11	0.67	0.80	0.43
Ganges	Asaraghat	360	0.95	0.11	0.79	0.84	0.59
	Kali Khola	201	0.93	0.11	0.66	0.79	0.79
	Chatara	344	0.93	0.13	0.65	0.70	0.77
Brahmaputra	Lazi	132	0.89	0.13	0.79	0.72	0.65
	Nugesha	181	0.92	0.15	0.46	0.56	0.54
	Lhasa	181	0.93	0.10	0.75	0.83	0.79
	Yangcun	169	0.94	0.10	0.77	0.82	0.80
	Nuxia	456	0.95	0.06	0.87	0.90	0.86
Salween	Jiayuqiao	460	0.93	0.13	0.68	0.72	0.87
	Gongshan	182	0.74	0.22	0.67	0.34	0.38
Mekong	Changdu	468	0.92	0.12	0.68	0.69	0.79
	Liutongjiang	76	0.94	0.16	0.57	0.63	0.79
Yangtze	Zhimenda	444	0.88	0.15	0.36	0.31	0.61
	Luning	240	0.95	0.12	0.56	0.67	0.72
Yellow	Tangnaihai	473	0.85	0.15	0.32	0.21	0.50
	Maqu	336	0.81	0.17	0.23	0.14	0.49

Asian water towers. In particular, high *CC* between the simulated and observed runoff is mainly attributed to the snow module that considers the lag between snowfall and melted water. Monthly runoff simulations in the Ganges and Brahmaputra water towers are also highly accurate. Despite glaciers on the Himalayas, the drainage basins of the Ganges and Brahmaputra water towers are highly impacted by the South Asia Monsoon and have a robust rainfall-runoff relationship, which serves as the basis for accurate model simulation. Atmospheric circulation across the Salween and Mekong water towers is also characterized by the South Asia Monsoon. However, narrow river channels in the lower reaches of these two basins, particularly the drainage basin at the Gongshan gauge, may impact the accuracy of the SM2R model. This is because ERA5L forcing data have a spatial resolution of 0.1° (~10 km), which might be too coarse to adequately reflect hydrologic characteristics here. As a result, we found generally good performance of SM2R-simulated runoff in the Salween-Mekong water towers, but the simulation results at the Gongshan gauge perform less well than at the other gauges. The lower reaches of the Yangtze and Yellow water towers are affected by the East Asia Monsoon, where the SM2R model also shows good performance (i.e., at the Luning gauge). However, headwaters of the Yangtze (the drainage basin at the Zhimenda gauge) and Yellow (drainage basins at the Maqu and Tangnaihai gauges) basins are located in the hinterland of the Tibetan Plateau, where the monsoon impacts are largely weakened. The headwaters of the Yangtze and Yellow basins are characterized by widely distributed permafrost and seasonally frozen soil, which may result in large uncertainties in soil moisture and soil texture estimation and therefore cause poor performance in simulated runoff at the Zhimenda, Maqu, and Tangnaihai gauges.

We separately examined scatterplots and time series of SM2R-simulated runoff at Gongshan, Zhimenda, Tangnaihai, and Maqu that have NSE < 0.5 (Figure 5). In situ observations are limited at the Gongshan gauge (182 in total; 84% complete over the recording period of 1999–2016), and the bias of individual simulations (e.g., the overestimation of SM2R-derived runoff during the summer months in 2014, Figure 5e) can impact the evaluation indices substantially in such small data samples. In addition, uncertainty in the forcing data due to the narrow drainage area at Gongshan gauge is another cause for the poor model performance. However, we find relatively

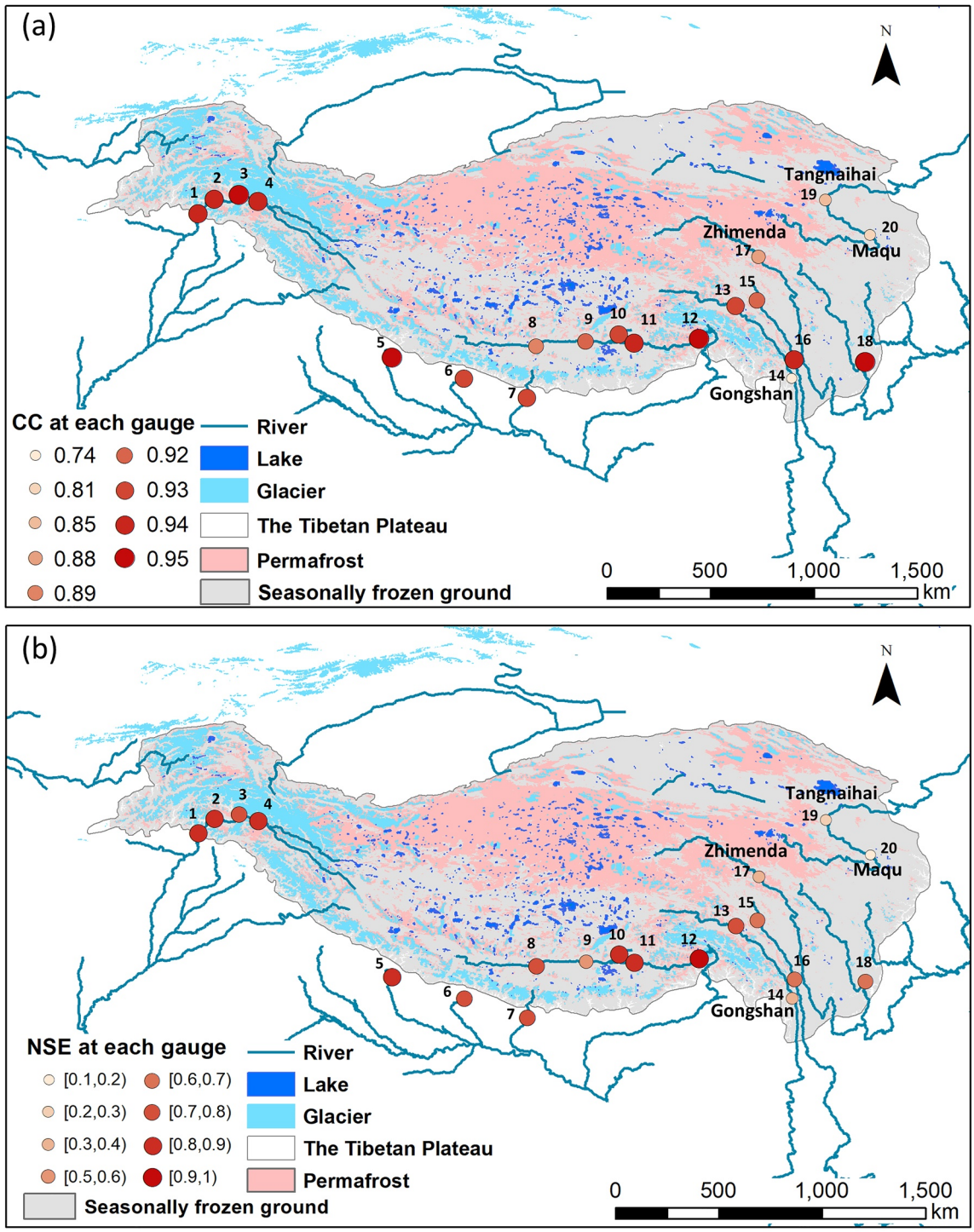

Figure 4. Spatial patterns of (a) CC and (b) NSE at each gauge over the seven Asian water towers. The darker and larger points show better performance at each gauge, whereas the lighter and smaller points show poorer performance.

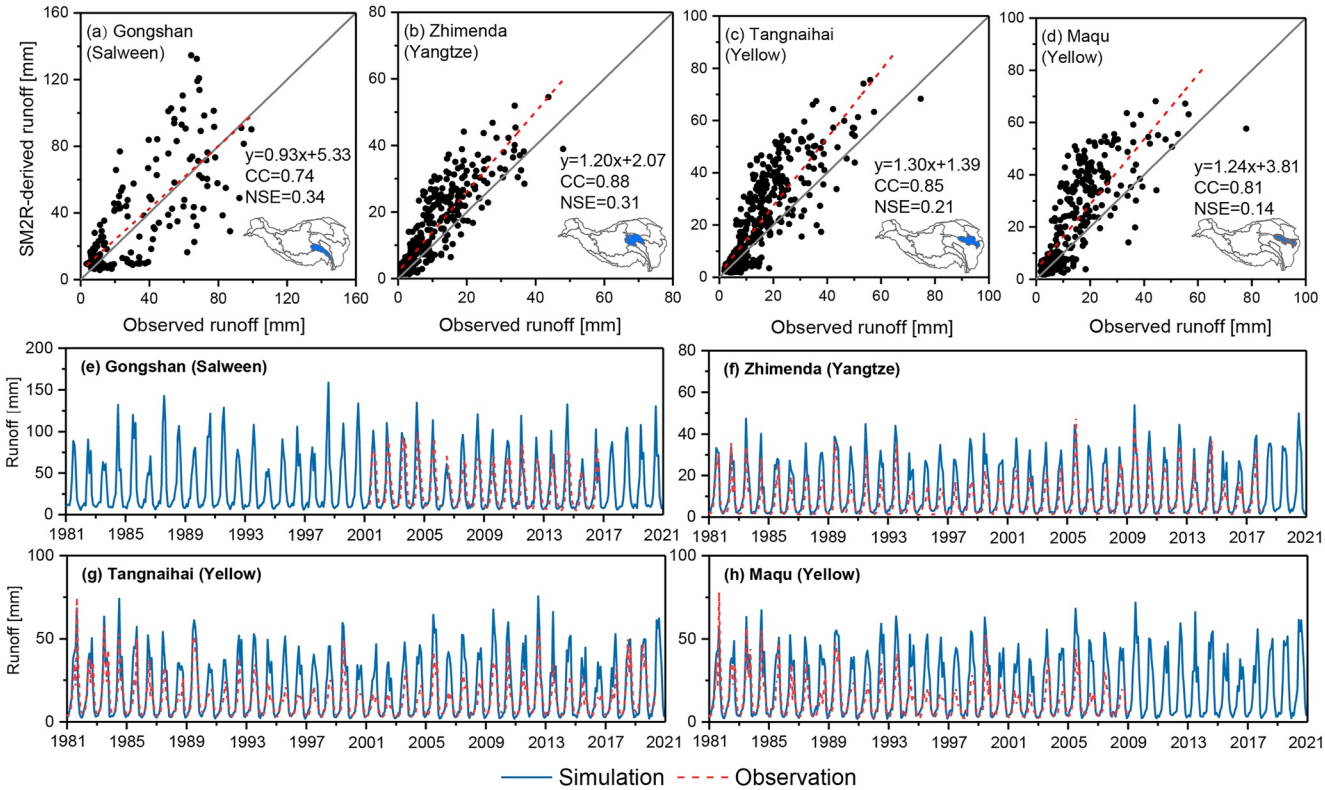

Figure 5. (a–d) Scatterplots and (e–h) time series of SM2R simulated and observed monthly runoff during 1981–2020 at the Gongshan, Zhimenda, Tangnaihai, and Maqu gauges. In (a–d), observed runoff is shown on the *x*-axis, whereas SM2R-derived runoff is shown on the *y*-axis. The 1:1 lines, linear fitting lines, regression equations, and evaluation indices of CC and NSE are also shown. Blue shaded regions shown in the bottom-right corner of panels (a–d) indicate the geographical locations of each drainage basin. In (e–h), SM2R simulated runoff is shown by solid blue lines, whereas observed runoff is shown by dashed red lines.

little difference between the linear regression line and 1:1 line in the scatterplots (Figure 5a), and high consistency between simulated and observed runoff in the annual and interannual variations (Figure 5e).

Observed runoff at the Zhimenda, Tangnaihai, and Maqu gauges is among the lowest magnitude of all drainage basins (Table 3), and we find an overestimation of SM2R-derived runoff at these gauges, particularly at the higher end (Figures 5b–5d). Specifically, the SM2R model overestimates summer high flows across these three drainage basins in dry years, for example, during 1994–1998, when observed runoff shows a sharp decline but

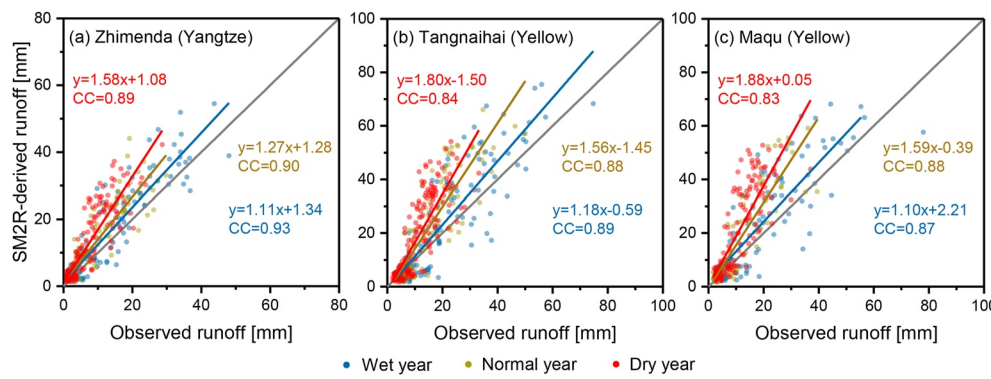

Figure 6. Scatterplots of SM2R simulated runoff and observed monthly runoff during wet, normal, and dry years during 1981–2020 at the (a) Zhimenda, (b) Tangnaihai, and (c) Maqu gauges. Observed runoff is shown on the *x*-axis, whereas SM2R-derived runoff is shown on the *y*-axis. The 1:1 lines, linear fitting lines, regression equations, and correlation coefficients (CC) between SM2R-derived and observed runoff are also shown. Results for wet, normal, and dry years are shown in blue, yellow, and red, respectively.

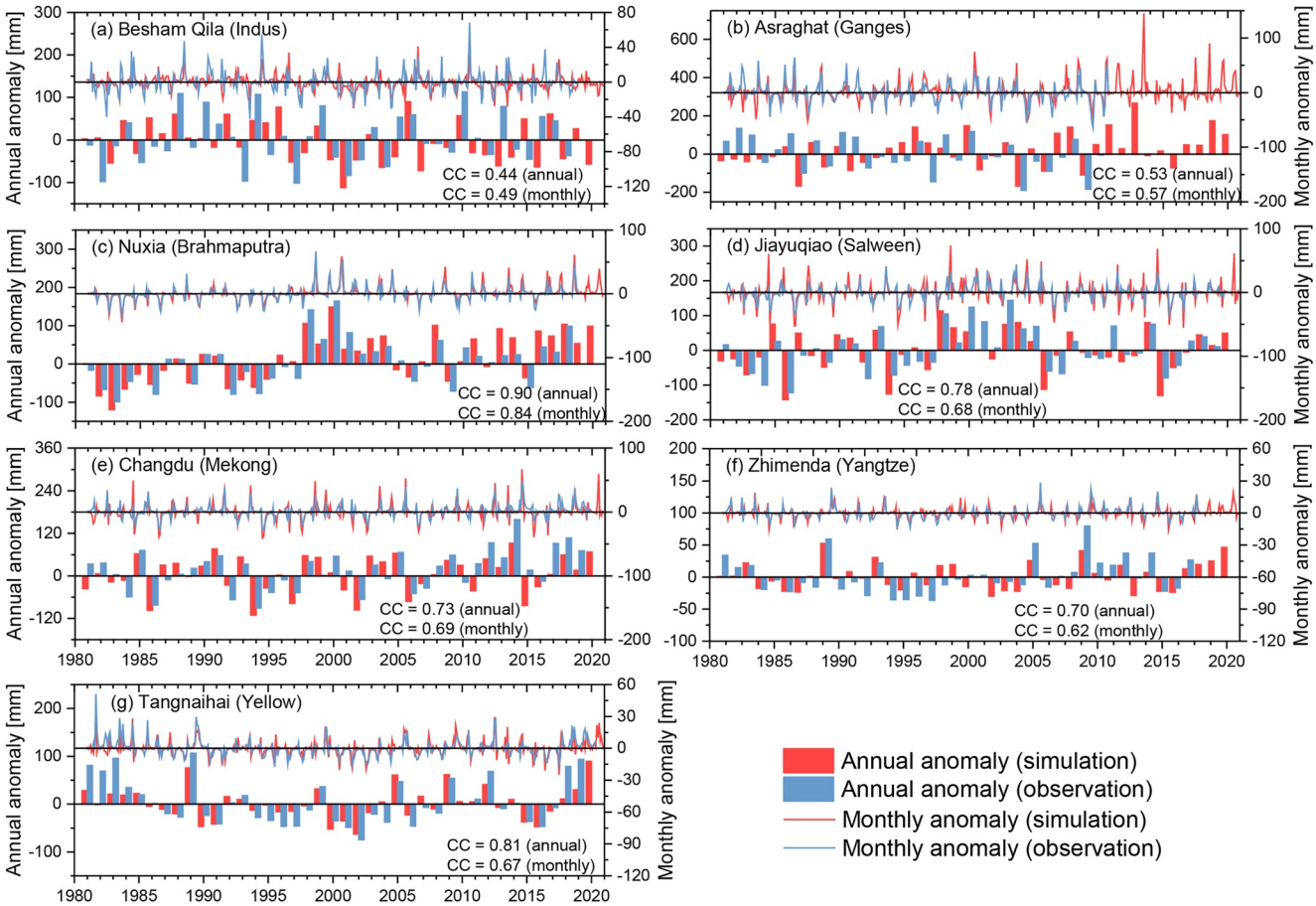

Figure 7. Evaluation of the SM2R model in simulating the anomaly both at the annual and monthly timescales. Annual anomalies are shown in bars on the left *y*-axis, and monthly anomalies are shown in lines on the right *y*-axis. SM2R-simulated anomalies are in red, whereas anomalies derived from runoff observations are in blue. Correlation coefficients (CC) between the observed and SM2R-simulated time series are also shown for each basin both at the annual and monthly timescales.

SM2R-derived runoff only slightly decreases (Figures 5f–5h) Separating the data into wet, normal, and dry years, that is, the percentage of the annual runoff anomaly to mean annual runoff is >10% (wet), −10%–10% (normal), and <−10% (dry), we find that the overestimation of SM2R-derived runoff is principally caused by simulations during dry years at the Zhimenda, Tangnaihai, and Maqu gauges (Figure 6). The overestimation during dry years results in the low evaluation indices across these three basins, which may be related to the complex rainfall-runoff relationship caused by frozen soil degradation here (Jin et al., 2009; Yang et al., 2004). During dry years when temperature is generally high, the intensified degradation of permafrost and seasonally frozen ground might increase soil water and soil evaporation. Along with the decrease in precipitation during dry years, precipitation may be increasingly partitioned into ET rather than runoff across regions with degradation of frozen soil. Moreover, soil porosity might also be larger after the degradation of frozen soil. Any changes in soil porosity may be another source of uncertainty for the SM2R model, because this variable is directly involved in runoff calculation. Although the SM2R model does not individually address uncertainties caused by the complex soil texture (see discussions in Section 5.2), the overall performance of SM2R-derived runoff is basically acceptable with CC > 0.8, NSE > 0, and logNSE > 0.49, which is much better than other models (see Section 4.3).

In addition, we evaluated SM2R by simulating the anomaly at both the annual and monthly timescales (Figure 7). We selected a representative drainage basin in each water tower with an observation period of at least 30 consecutive years to provide a reliable climatological normal. In general, the SM2R model performs well in simulating anomalies across the seven water towers, showing high *CC* between the observed and simulated anomalies (*CC* > 0.44 for the annual timescale and CC > 0.49 for the monthly timescale). Consistency between simulated and observed anomalies in the monsoon-dominated basins (e.g., the Ganges, Brahmaputra, Salween, and Mekong water towers; Figures 7b–7e) is higher than in the Indus water tower (Figure 7a). In particular, the Brahmaputra

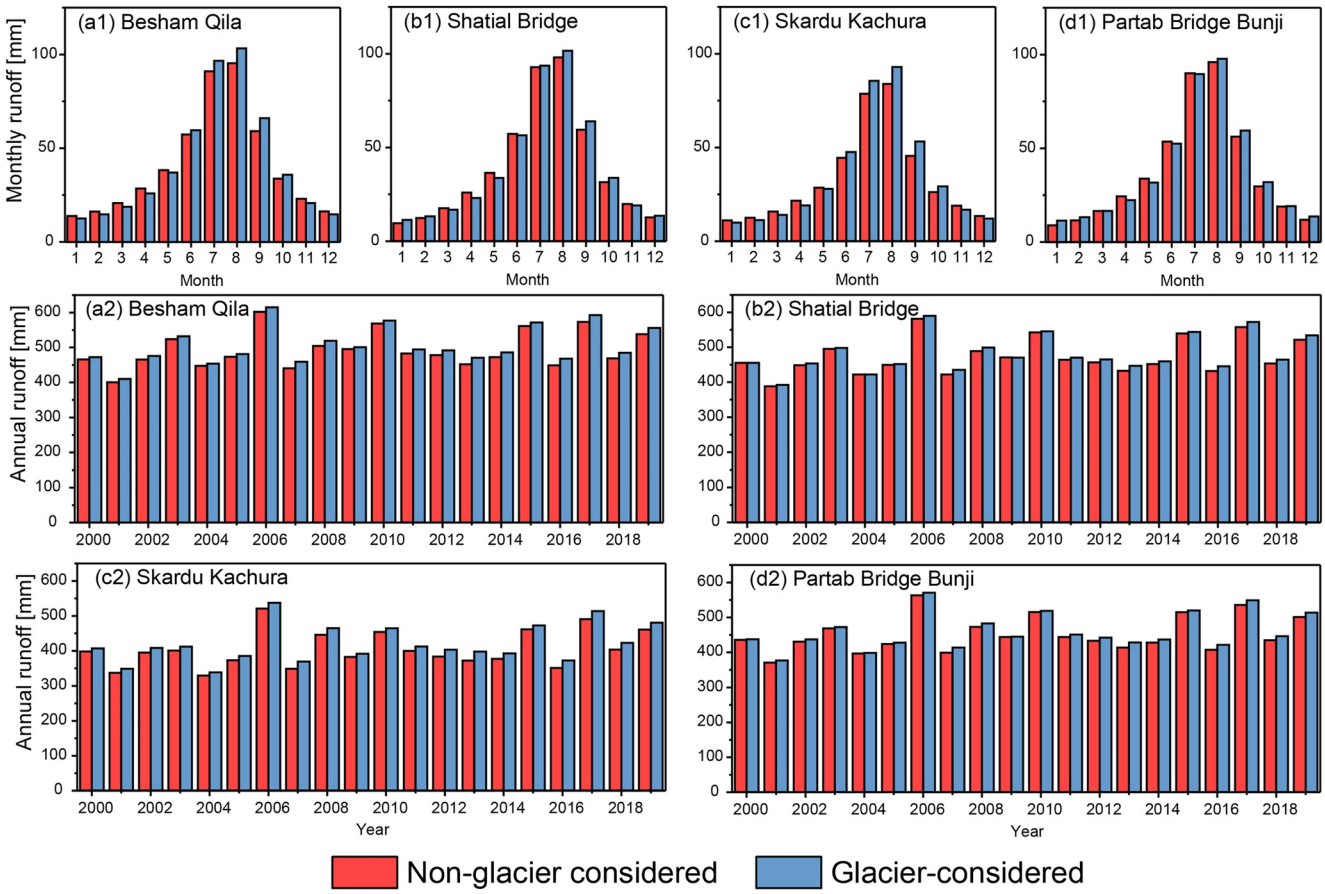

Figure 8. (a1–d1) Mean monthly (a2–d2) annual runoff simulated by the SM2R model across four drainage basins in the Indus water tower during 2000–2019. Red bars show runoff simulation without the glacier module, whereas blue bars show runoff simulation with the glacier module.

basin shows the highest degree of accuracy with CC = 0.84 and 0.90 for the monthly and annual anomalies, respectively (Figure 7 (c)). Good performance over the monsoon-dominated basins is possibly attributed to the robust rainfall-runoff relationship, which serves as the basis for SM2R simulation. In contrast, relatively poor performance in the Indus water tower may be caused by complex cryospheric processes, where the widely distributed glaciers, snow, and permafrost may increase the challenge in accurately simulating anomalies. It is promising that at the Zhimenda (Figure 7f) and Tangnaihai (Figure 7g) gauges, the SM2R model shows high reliability in estimating positive and negative anomalies, despite that evaluation indices at these two gauges do not perform as well as at the other 16 gauges over the Asian water towers. High CC between simulated and observed anomalies in both monthly (>0.62) and annual (>0.70) timescales indicates that the SM2R model can capture variability well over these two basins, although the magnitude requires attention particularly in dry years (Figure 6).

4.2. Impacts of Net Glacier Mass Changes on Runoff Estimation

Due to the limited accessibility of data on glacier mass changes, the glacier module is implemented only during the 2000–2019 period in this study. To examine the impacts of net glacier mass changes on runoff simulation, here we compare runoff that is simulated with and without the glacier module across four drainage basins in the Indus water tower during 2000–2019 (Figure 8). At the mean monthly timescale (Figures 8a1–8d1), the supplemented glacier module in the SM2R model results in slightly higher runoff estimation during July–September but slightly lower runoff estimation during March–May. This is generally consistent with past studies on Indus runoff analysis using hydrologic models, which indicated that the glacier meltwater mostly increased in July and peaked in August (Biemans et al., 2019), but did not play a key role during March–May when snowmelt was the maximum within a year (Kraaijenbrink et al., 2021). At the annual timescale (Figures 8a2–8d2), glacier mass loss

Table 7
Specific Values of NSE, logNSE, CC, NRMSE, and KGE Evaluating ERA5L-Derived Runoff Based on Observations From 20 Gauges

Basin	Gauge	Observations (months)	CC	NRMSE	KGE	NSE	logNSE
Indus	Besham Qila	456	0.71	0.19	0.60	0.35	0.14
	Shatial Bridge	204	0.69	0.20	0.49	0.31	−0.07
	Partab Bridge Bunji	300	0.71	0.24	0.57	0.17	0.18
	Skardu Kachura	444	0.67	0.22	0.56	0.25	−0.06
Ganges	Asaraghat	360	0.84	0.15	0.84	0.68	0.76
	Kali Khola	201	0.90	0.11	0.78	0.80	0.83
	Chatara	344	0.91	0.19	0.44	0.42	0.75
Brahmaputra	Lazi	132	0.81	0.19	0.54	0.40	0.30
	Nugesha	181	0.91	0.12	0.59	0.70	0.45
	Lhasa	181	0.90	0.13	0.62	0.73	0.36
	Yangcun	169	0.94	0.13	0.61	0.72	0.53
	Nuxia	456	0.95	0.07	0.74	0.85	0.68
Salween	Jiayuqiao	460	0.91	0.17	0.53	0.57	0.47
	Gongshan	182	0.63	0.99	−1.88	−12.00	−1.51
Mekong	Changdu	468	0.86	0.17	0.51	0.38	0.37
	Liutongjiang	76	0.92	0.18	0.59	0.56	0.48
Yangtze	Zhimenda	444	0.91	0.30	−0.60	−1.71	−0.23
	Luning	240	0.96	0.13	0.53	0.63	0.51
Yellow	Tangnaihai	473	0.73	0.92	−4.15	−34.31	−2.91
	Maqu	336	0.77	0.27	−0.41	−2.24	−0.88

provides additional water into the soil system, and thus causes slightly larger runoff in each year compared to the simulations without the glacier module.

However, we find only minor differences in runoff estimation caused by net glacier mass changes, that is, mean annual runoff during 2000–2019 increased slightly by 1.5%–3.8% across the four drainage basins if considering the glacier module. Two major reasons contribute to such slight differences. First, despite much higher glacier concentration in the Indus water tower than others, in this study additional water provided by net glacier mass changes is minor compared to the amount of precipitation at the basin scale. Taking the drainage basin at the Shatial Bridge gauge as an example, the rate of glacier retreat during 2000–2019 was −0.12 m w.e./yr (the glacier area is 19,621 km^2), which equals an additional water input of 11 mm/yr for the entire drainage basin (the basin area is 183,119 km^2). However, mean annual precipitation in this drainage basin is ∼550 mm/yr, which is 50 times larger than the additional water input provided by net glacier mass changes. Second, although some studies on runoff component analysis declared a large contribution of glacier runoff to total runoff in the Indus water tower (Biemans et al., 2019; Lutz et al., 2014), these studies defined glacier runoff as runoff generated by net glacier mass changes and precipitation on the glaciers. In this study, the glacier module only represents runoff caused by net glacier mass changes, whereas runoff caused by precipitation on glaciers (i.e., the major contribution to glacier runoff in hydrologic models), is already included in the estimation of basin-averaged runoff (see Section 5.2 for more detailed discussion). Overall, the absence of the glacier module due to data availability only produces a minor difference, but as illustrated before, the proposed glacier module plays a significant role in understanding and guiding runoff generation over other glacier-dominated basins.

4.3. Comparisons Between SM2R and ERA5L-Derived Runoff Estimation

Monthly runoff estimation during the 1981–2020 period derived from ERA5L, which provides major forcings in this study, is evaluated at 20 gauges to show applicability of the reanalysis model over the Asian water towers (Table 7 and Figure 9). Although the evaluation indices of ERA5L and SM2R models are comparable at the Kali

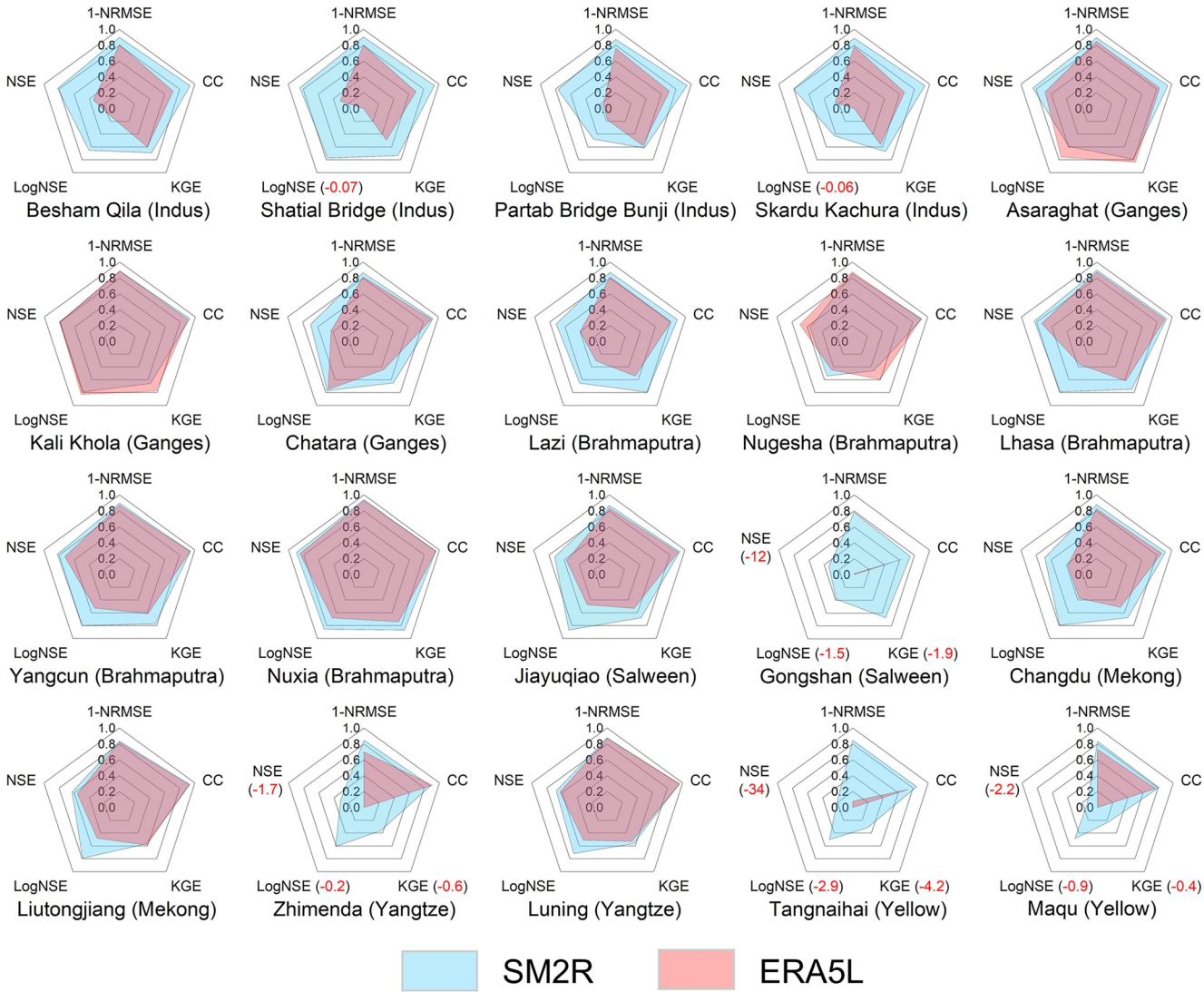

Figure 9. Radar plots of five indices (i.e., NSE, logNSE, CC, NRMSE, and KGE) evaluating SM2R and ERA5L-derived runoff based on observations from 20 gauges. Evaluation results from SM2R are shown in blue, whereas those from ERA5L are shown in red. Indices of ERA5L evaluation with values < 0 are excluded in the plots but the values are specifically provided in red font (at the Shatial Bridge, Skardu Kachura, Zhimenda, Tangnaihai, and Maqu gauges). The NRMSE index is shown as (1-NRMSE) in the plots, and a perfect fit is indicated by a value of 1 for all indices.

Khola and Nugesha gauges, the accuracy of estimated runoff from ERA5L is much lower than that of SM2R at other 18 gauges. It seems that the ERA5L runoff may be useful in monsoon-dominated regions, for example, the Ganges and Brahmaputra water towers. However, ERA5L-derived runoff shows rather poor applicability in the Indus water tower that is heavily impacted by cryospheric processes (NSE = 0.17–0.35), and is unreliable in headwaters of the Yangtze and Yellow basins that are undergoing intense degradation of frozen soil (NSE < 0) (Table 7).

Here we further show comparisons between ERA5L and SM2R simulated runoff at eight gauges over the Indus, Salween, Yangtze, and Yellow water towers (Figure 10). ERA5L-estimated runoff substantially diverges from the 1:1 line in the scatterplots compared to observed runoff in the Indus water tower, particularly in the high end (Figures 10a–10d). Compared to ERA5L, the proposed SM2R model largely improves the correlation and reduces discrepancies for runoff estimation in the Indus water tower (CC = 0.94–0.95 for SM2R vs. 0.67–0.71 for ERA5L estimation; $NRMSE$ = 0.10–0.13 for SM2R vs. 0.19–0.24 for ERA5L estimation; Tables 6 and 7), such that simulated runoff more closely follows the 1:1 line in the scatterplots (Figures 10a–10d). A major limitation of the ERA5L runoff in the Indus water tower is the misunderstanding of monthly runoff distribution, that is, the

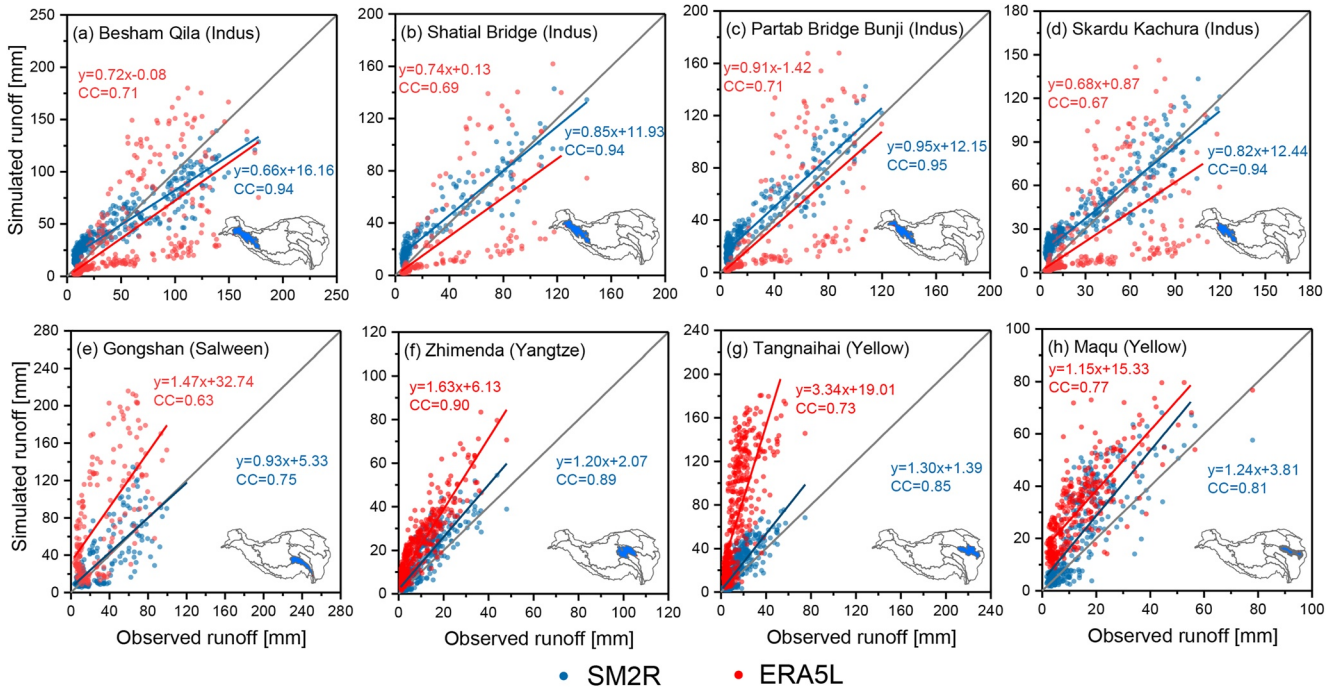

Figure 10. Scatterplots of simulated and observed monthly runoff during 1981–2020 at gauges of the Indus, Salween, Yangtze, and Yellow water towers. Observed runoff is shown on the *x*-axis, whereas model-derived runoff is shown on the *y*-axis. The 1:1 lines are also shown. Scatterplots, linear regression lines, and linear regression equations of the SM2R model are shown in blue, whereas those from the ERA5L runoff are shown in red. Shadow regions of the inserted boundary on the bottom-right corner denote geographical locations of each drainage basin.

mean monthly peak of ERA5L-derived runoff (in June) is shown to be 1-month earlier than the peak of observed runoff (in July) (Figure 11a–11d).

At Gongshan, Zhimenda, Tangnaihai, and Maqu gauges where the SM2R model does not perform as well as other 16 gauges, the ERA5L-derived runoff performs much more poorly, with $NSE < 0$. Large overestimation of

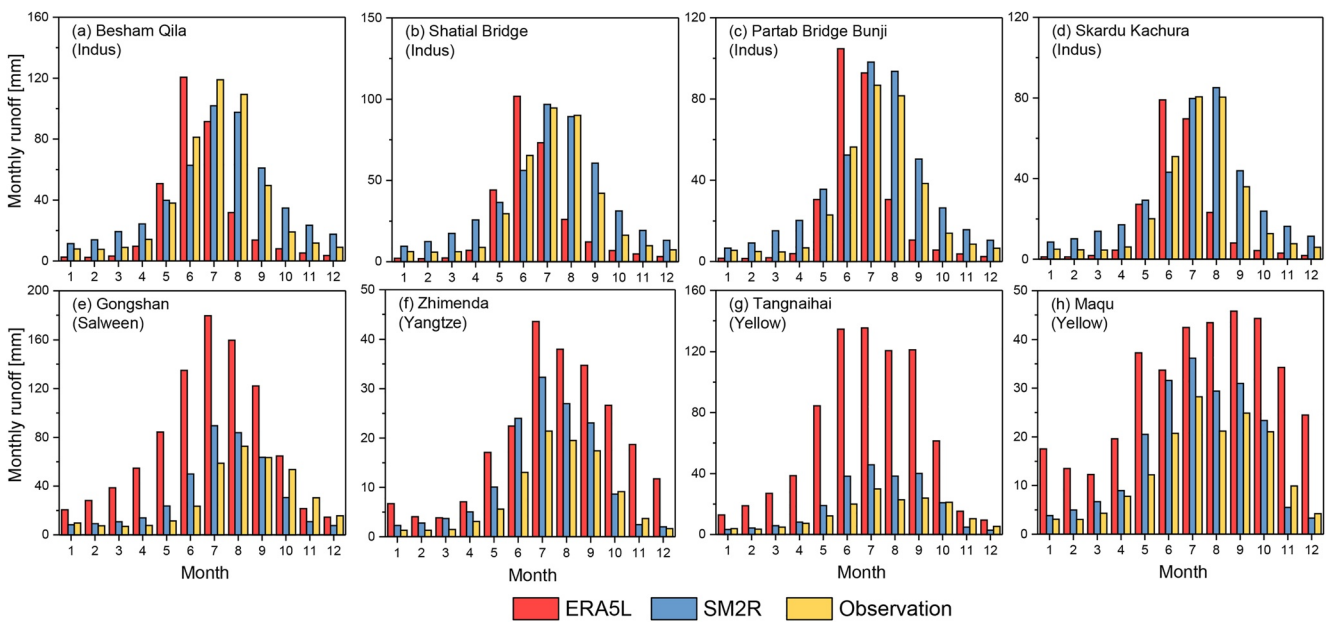

Figure 11. Mean monthly runoff estimated from the ERA5L (red bars), SM2R (blue bars), and in-situ observations (yellow bars) at eight gauges.

ERA5L-derived runoff represents the major weakness of the reanalysis model (Figures 10e–10h) in these four drainage basins. Such overestimation of the ERA5L runoff occurs in each month, and requires particular caution during monsoon months (May–September) (Figures 11e–11h). Using changes in VSM to constrain the model, SM2R-derived runoff reduces the overall simulation bias at these four gauges (NRMSE = 0.15–0.22 for SM2R vs. 0.27–0.99 for ERA5L estimation; Tables 6 and 7), which makes the regression lines approach to the perfect 1:1 lines in the scatterplots (Figures 10e–10h).

5. Discussion

5.1. Major Advantages of the Proposed SM2R Model

We summarize the advantages of the proposed SM2R model on the following three aspects. First, this model does not invoke any in-situ runoff observations, showing considerable potential for runoff analysis across poorly gauged and ungauged regions. Although past studies have developed different runoff model structures, SM2R is in a preliminary attempt to estimate basin-scale runoff from the knowledge of soil moisture information and independently from any observed runoff calibration. Ghajarnia et al. (2020) evaluated variations in hydrologic variables in more than 1,000 drainage basins across Europe during 1980–2010, and found a robust correlation not only between monthly soil moisture and monthly runoff, but also between extreme soil moisture and runoff. This supports the key message that soil moisture information has considerable potential to provide additional constraints on runoff estimation. In particular, the coupled snow and glacier modules in the SM2R model strengthen the model's applicability across cryospheric regions that were generally excluded by the previous SM2RAIN structure (Brocca et al., 2013; Brocca et al., 2015; Ciabatta et al., 2018). To the best of our knowledge, this study provides the most comprehensive evaluation of runoff simulation at 20 gauges across seven Asian water towers with different geographic and climate characteristics. Findings from this study show new insights in PUB, which is particularly valuable over ungauged global water towers impacting water availability for about 22% of the global population (Immerzeel et al., 2020).

Second, compared with hydrologic or land surface models, this approach is minimalistic in both the required forcing data and model parameters. The SM2R model is forced using three key variables (precipitation, PET, and VSM) from the global reanalysis ERA5L data, along with some additional information from soil texture, snow, and glaciers. Only seven independent parameters must be optimized and determined, the number of which is much smaller than other hydrologic or land surface models. Here we take a hydrologic model, Coupled Routing and Excess Storage Model-Snow (CREST-Snow) as a comparison. The original version of CREST-Snow, CREST, was a distributed hydrological model jointly developed by the University of Oklahoma and NASA SERVIR (Wang et al., 2011). CREST-Snow is an advanced version that coupled a snow and glacier module with CREST to improve its applicability in cryospheric regions (Chen et al., 2017), which has been widely used in runoff estimation and has achieved promising results over the Asian water towers (P. Han, Long, Fang, et al., 2019; Z. Han, Long, Fang, et al., 2019; Z. Han et al., 2020; Huang et al., 2020). Twenty-four parameters are required in CREST-Snow, including 16 parameters for runoff generation, 6 parameters in the snow module and two parameters in the glacier module. The large number of parameters increases the risk of equifinality, and requires more essentially accurate observations to constrain the model results and improve the model performance and parameter reasonability. For example, CREST-Snow jointly uses observed runoff, observed/remote sensing-based snow water depth, remote sensing-based SCA, snow water equivalent, and terrestrial water storage changes to fully calibrate the model parameters. In contrast with most hydrologic models or LSMs, the minimalistic parameters in the SM2R model can largely reduce the uncertainty arising from equifinality and data inconsistency.

Third, appropriate mathematical functions of the relationships between flux variables and VSM largely improve model performance. Here we compare our study with Koster et al. (2018), who implemented a simple linear relationship between runoff and soil moisture to estimate basin-scale runoff at the 10-day timescale during the warm seasons in 2015–2017. Koster et al. (2018) assumed that fast runoff was proportional to the product of precipitation (P) and soil moisture (SM), whereas slow runoff was directly proportional to soil moisture, given by Equation 26.

$$R = R_{\text{fast}} + R_{\text{show}} = p_1 \cdot P \cdot \text{SM} + p_2 \cdot \text{SM} + p_3 \tag{26}$$

To determine the three parameters, that is, p_1, p_2, and p_3 in Equation 26, Koster et al. (2018) used observed precipitation and satellite-based soil moisture as the input, and relied on two thirds of observed runoff to calibrate this linear regression relationship (i.e., selecting 2 years during 2015–2017 for calibration and the other 1 year for

validation). Although calibrated by observed runoff, only 22 of 145 examined basins in the United States had a coefficient of determination (r^2) > 0.5 (corresponding to CC > 0.71), which performed less well than the results in our study (all examined gauges had r^2 > 0.5). In addition, the study period in Koster et al. (2018), that is, only warm seasons during 2015–2017 was much shorter than that of our study, that is, 40 years in total. Relatively poor performance in Koster et al. (2018) may be attributed to the simple linear regression that may not accurately reveal the interaction between soil moisture and runoff. In addition, the above study did not involve a full consideration of water balance, particularly glacier and snow impact on runoff generation. Compared with Koster et al. (2018), this study largely improves the model structure and performance, showing the benefits of exploring relationships between soil moisture and runoff.

5.2. Caveats and Limitations

One caveat of the SM2R model is that it may not perform well at the daily or hourly timescale. This is because SM2R-derived runoff depends on the relationship between equivalent water input and soil moisture (Equations 15 and 16), which may not be sufficiently robust at the daily or hourly timescale. Basin-averaged daily runoff lags behind daily precipitation, and an additional runoff routing system is necessary for high-temporal estimates. Therefore, this approach is likely to be more applicable for estimating long-term runoff variations at the monthly timescale than for analyses of high temporal resolution.

Soil information serves as the foundation to estimate runoff and, thus, accuracy of the SM2R model may be lower in regions with complex soil texture (e.g., headwaters of the Yangtze and Yellow river basins that show frozen soil degradation) than other drainage basins. Most root-zone soil moisture estimates, for example, ERA5L, SMAP-L4 (Soil Moisture Active Passive L3), and LSM results from GLDAS (Global Land Data Assimilation System), show large uncertainty in soil moisture variations during the freezing/thawing period over frozen regions (Xing et al., 2021). In addition, degradation of permafrost and seasonally frozen ground may increase soil water capacity, whose impacts on surface and subsurface runoff and soil evaporation are non-linear and complicated. Moreover, basin-scale soil porosity is larger after frozen soil degradation, and the uncertainty of porosity is directly related to runoff, as well as ET and drainage estimation (Equations 11, and 14–16). Therefore, uncertainties in ERA5L-based VSM and HSWD-based soil texture data combined with complex relationships between soil moisture and runoff process may translate to poor performance of the SM2R model over frozen regions. We acknowledge that more efforts are required in understanding the impacts of frozen soil thawing/freezing on runoff generation processes, and more representative soil texture data sets are necessary to improve runoff estimation over permafrost regions. However, this study mainly focuses on using available soil information to estimate runoff, and the task of improving accuracy of available soil data sets is out of scope.

It is worth noting the difference between P_{Eq} in glacier and snow modules and snow/glacier melt water. SM2R is a lumped model that uses basin-averaged estimates as forcings instead of distinguishing spatial variability in precipitation across snow/glacier covered areas. In SM2R, P_{Eq} represents the basin-averaged equivalent water input for the soil system, which can cause changes in soil moisture and regulate ET, drainage, and runoff. The glacier module considers the contribution from net glacier mass changes to soil water input, and the snow module shows the time lag of snowfall melting to liquid water. In contrast, in most hydrologic models, the glacier (snow) melt water is defined as runoff generated across the glacierized (snow-covered) areas, including runoff caused by not only net glacier mass changes (melted snowfall), but also large precipitation on glaciers (snow-covered areas). Therefore, this study does not explicitly calculate contributions from different runoff components as defined in hydrologic models. Instead, we consider the impacts of net glacier mass changes and melted snowfall individually, and input basin-averaged precipitation to force the model.

5.3. On the Forcing Data

Notwithstanding substantial progress in observational instrumentation, satellite retrievals, and modeling, accurate estimation of hydrologic variables over the Asian water towers is challenging due to the complex terrains, sparse in situ observations, and a harsh environment. Past studies (Cheng et al., 2019; Xing et al., 2021) have assessed the accuracy of model-based soil moisture estimation (e.g., soil moisture derived from ERA5L, SMAP, and LSMs) based on gauge observations on the Tibetan Plateau, but evaluation results are not consistent across these studies due to differences between model-defined and observed soil moisture depth. Compared with the

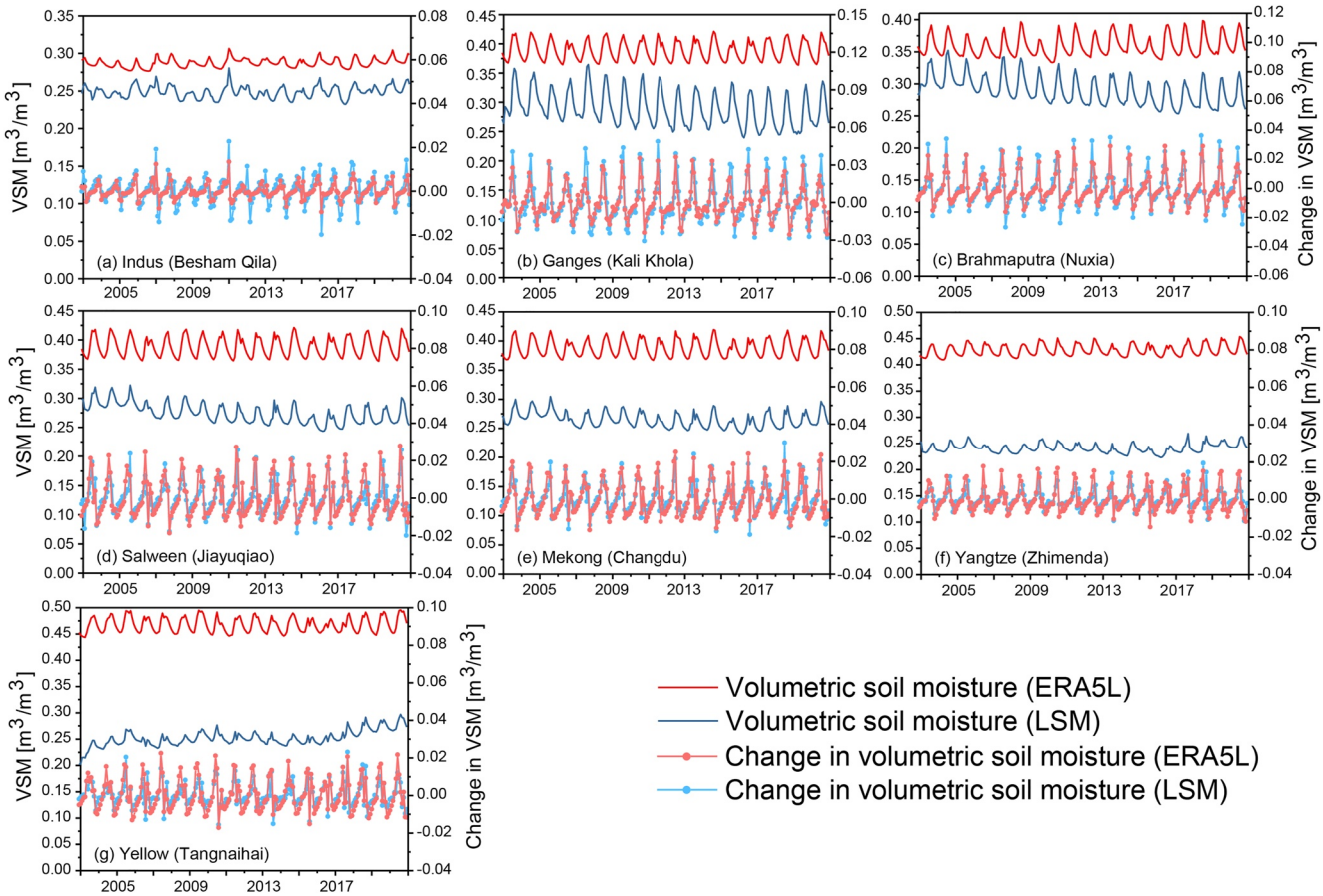

Figure 12. Monthly VSM and changes in VSM estimated from ERA5L and LSM (the average of NOAH and CLSM) during 2003–2020 across the selected drainage basin in each Asian water tower. Red and blue lines show VSM estimated from ERA5L and LSM, respectively, on the left *y*-axis. Red and blue lines with dots show changes in VSM estimated from ERA5L and LSM, respectively, on the right *y*-axis.

storage variable (soil moisture), hydrologic fluxes have larger uncertainty, which may cause non-closure in water balance, particularly over high-elevation regions where ground observations/gridded estimates show rather limited representativeness. For example, Immerzeel et al. (2015) indicated that in the upper Indus basin, the amount of precipitation required to sustain the observed mass changes of large glacier systems should be far beyond the values observed at valley stations or estimated by gridded precipitation products (up to twice to 10 times).

In this study, the latest global ERA5L reanalysis data provide major inputs for the SM2R model, including VSM, precipitation (snowfall and rainfall), and PET. Due to challenges in obtaining an accurate forcing baseline, we did not individually evaluate each forcing variable from ERA5L based on in-situ observations. Instead, here we illustrate the reliability and robustness of the SM2R model by analyzing the accuracy of changes in VSM, the effective constraint on runoff estimation, and the independent calculation of different hydrologic fluxes.

First, a reliable estimation of changes in VSM directly determines the objective function (Equation 18), and therefore is fundamental to constrain the SM2R model. We selected a drainage basin in each water tower to compare VSM and changes in VSM estimated from the ERA5L and LSMs (the average of NOAH-3.6 and CLSM-F2.5 from GLDAS) during the overlapping period of 2003–2020 (Figure 12). Although discrepancy in the magnitude of VSM exists, we find high consistency between the ERA5L and LSM-derived changes in VSM. Mean biases between ERA5L and LSM-derived VSM over the examined basins are 0.039 (Indus), 0.078 (Ganges), 0.070 (Brahmaputra), 0.114 (Salween), 0.123 (Mekong), 0.187 (Yangtze), and 0.216 (Yellow) m^3/m^3. Such bias may be attributed to estimation uncertainty and different vertical levels of soil depth in each model output, that is, 0–289 cm for ERA5L, 0–200 cm for NOAH, and 0–100 cm for CLSM. However, mean bias in changes in VSM approaches 0 in all examined basins, indicating consensus in capturing soil moisture variations from different models. Because changes in VSM are

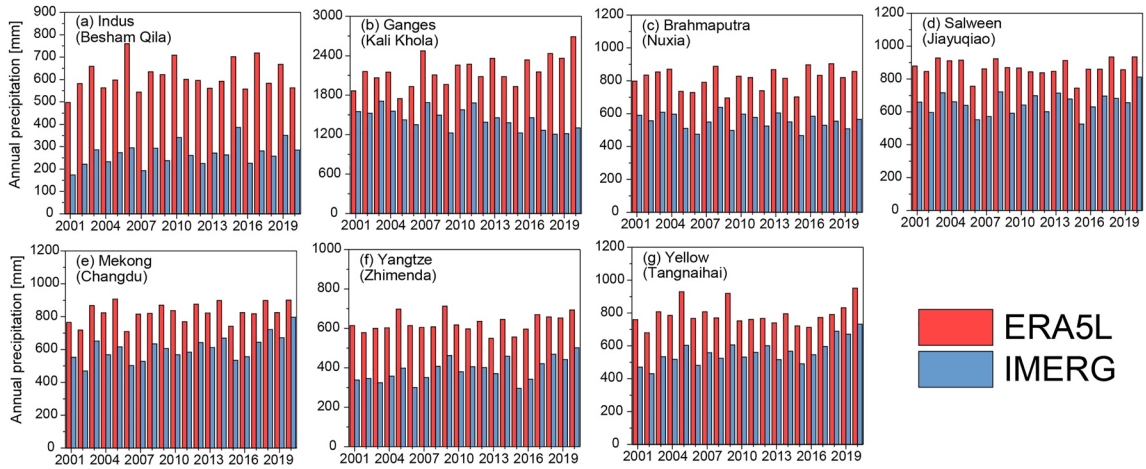

Figure 13. Annual precipitation estimated from reanalysis-based ERA5L and satellite-based IMERG during 2001–2020 (the overlapping period for the two data sets) over the representative drainage basins in each water tower.

directly involved in the objective function to constrain the SM2R model, the reliability and accuracy of VSM variations could provide a promising way to optimize model parameters and largely support the reliability of SM2R.

Second, the effective constraint on runoff estimation is found based on reliable changes in VSM. Here we compared SM2R-derived runoff using two different precipitation inputs, that is, reanalysis-based ERA5L and satellite-based Integrated Multi-satellitE Retrievals for GPM (IMERG) during the overlapping period of 2001–2020. Despite similar annual variability, difference in annual precipitation estimated from ERA5L and IMERG is 200–740 mm across seven Asian water towers (Figure 13), which is particularly large in the Indus (350 mm) and Ganges (740 mm) basins. The satellite-based IMERG product seems to largely underestimate precipitation in the Indus and Ganges basins (270 mm in the Indus and 1445 mm in the Ganges basin), given the observed runoff values (475 mm at Besham Qila and 1763 mm at Kali Khola station). With the exception of the Indus and Ganges water towers where IMERG precipitation is low, SM2R-derived runoff shows high consistency across drainage basins in the five other water towers (Figure 14). This indicates that large discrepancies in precipitation may be reduced through parameter optimization that depends on the effective constraint through reliable changes in VSM, which further supports the reliability and robustness of the SM2R model.

Third, hydrologic fluxes in the SM2R model are calculated independently, indicating that uncertainty in each kind of forcing variable can be limited to the related function. For example, different precipitation forcings only impact differences in runoff and the parameter e by Equation 15, but show little impacts on parameters related to ET and drainage estimation. Such independence reduces the risk of equifinality, providing a robust model structure for

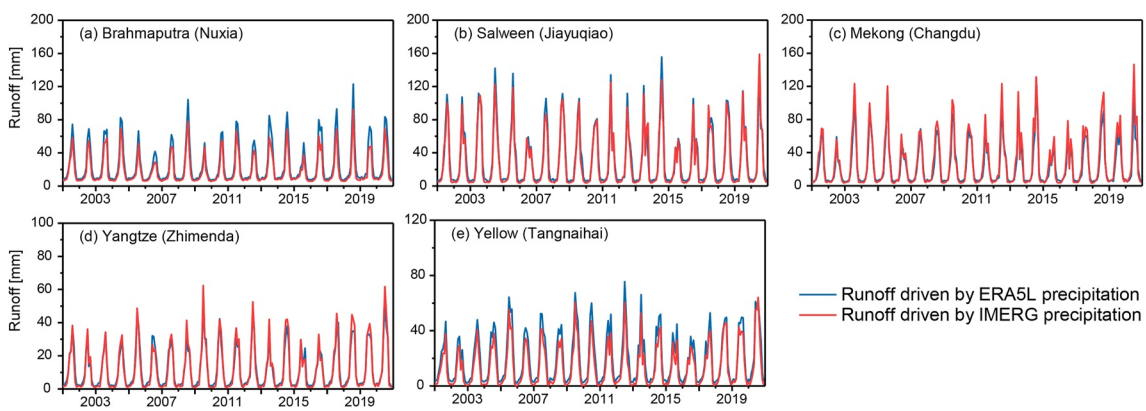

Figure 14. SM2R-estimated monthly runoff forced by ERA5L (blue lines) and IMERG (red lines) precipitation during 2001–2020 across the drainage basins in the (a) Brahmaputra, (b) Salween, (c) Mekong, (d) Yangtze, and (e) Yellow water towers.

Table 8
Differences in Parameters Related to ET (a) and Drainage (b and c) Using Precipitation Forcing Derived by ERA5L and IMERG

Water tower	Outlet gauge	Precipitation input	*a*	*b*	*c*
Brahmaputra	Nuxia	ERA5L	6.03	13.11	15.77
		IMERG	6.18	13.07	15.83
Salween	Jiayuqiao	ERA5L	5.62	60.35	11.46
		IMERG	5.62	60.28	11.75
Mekong	Changdu	ERA5L	5.78	60.15	12.28
		IMERG	5.74	60.16	12.25
Yangtze	Zhimenda	ERA5L	6.07	25.57	12.48
		IMERG	6.16	25.53	12.62
Yellow	Tangnaihai	ERA5L	5.76	25.74	11.85
		IMERG	5.95	25.68	12.09

water balance components. To further illustrate this, we compared differences in parameters related to ET (*a* in Equation 11) and drainage (*b* and *c* in Equation 14) using ERA5L and IMERG precipitation to force the SM2R model, and found very slight differences from changing the precipitation forcing (Table 8). The robustness of these parameters indicates that the estimation of ET and drainage is slightly impacted by the precipitation forcing, which further shows that uncertainty in individual forcings does not translate to all components estimated in the SM2R model.

Overall, despite challenges in estimating accurate hydrologic forcings over the high-mountain Asian water towers, we find highly consistent changes in VSM among different models, which provides a reliable and fundamental constraint for the SM2R model. Consistent runoff is estimated using different precipitation forcings, indicating the effectiveness of parameter optimization constrained by changes in VSM. In addition, uncertainty in each kind of forcing can be limited to the estimation of a specific component rather than translate to all components in the SM2R model. These points support the reliability and robustness of the SM2R model, which provides a promising approach to constrain flux estimation using information from soil moisture.

6. Conclusions

This study proposes a data driven model, SM2R, to estimate long-term runoff from soil moisture dynamics. The approach is minimalistic, robust, and independent of any observed runoff for calibration. Twenty drainage basins across seven poorly-gauged Asian water towers were examined during the past four decades (1981–2020). To the best of our knowledge, this analysis provides the most comprehensive evaluation of long-term runoff variations to date for the Asian water towers. Relatively high correlation and low variance between SM2R-derived and observed monthly runoff are found at all gauges (CC $\geq$ 0.74 and NRMSE $\leq$ 0.22). The more comprehensive NSE and KGE indices perform well at most gauges (NSE > 0.56 and KGE > 0.46 at 16 gauges), indicating considerable potential for runoff estimation in poorly-gauged and/or ungauged basins. Relatively low NSE and KGE values were found in basins with long and narrow drainage areas and widespread frozen ground, where the forcing data, particularly soil dynamics, may have large uncertainties.

Although the SM2R model is forced by ERA5L data in this study, runoff estimated from SM2R greatly outperforms that of the existing ERA5L runoff reanalysis. In particular, substantial improvements of SM2R-derived runoff occur in the Indus water tower which has high glacier concentration (NSE = 0.77–0.85 for SM2R simulation vs. 0.17–0.35 for ERA5L estimation), and in the headwaters of the Yangtze and Yellow basins, which have widely distributed frozen soil (NSE = 0.14–0.31 for SM2R simulation vs. −34.31–−1.71 for ERA5L estimation). Without invoking any observations for calibration, we find that the key variable in constraining model parameters (i.e., changes in VSM) has the least uncertainty among forcing variables, and explains the reliability and good performance of the SM2R model.

The application of soil moisture information to derive hydrologic fluxes is in its infancy. This study is a preliminary attempt to examine the potential of estimating basin-scale runoff using soil moisture, without requiring observations for calibration. The good performance of the proposed SM2R model across the high-mountain Asian water towers has valuable implications for understanding water security over this poorly-gauged region with complex terrain and climate. Moreover, no regional constraints are implemented in the SM2R model functions or forcing data. This new approach may be applied to other water towers globally, providing valuable information for PUB and water resources management.

Data Availability Statement

ERA5L reanalysis data (Muñoz Sabater, 2019) are available at https://cds.climate.copernicus.eu/cdsapp#!/dataset/10.24381/cds.68d2bb30. Data sets from the HWSD (Fischer et al., 2008) are accessed at https://www.fao.org/soils-portal/data-hub/soil-maps-and-databases/harmonized-world-soil-database-v12/en/. Glacier elevation changes (Berthier et al., 2021) are provided at https://doi.org/10.6096/13, and the RGI 6.0 glacier mask (RGI

Consortium, 2017) can be accessed at https://doi.org/10.7265/4m1f-gd79. Percentages of persistent snow cover in each water tower (Immerzeel et al., 2019) are provided at https://doi.org/10.5281/zenodo.3521933. Soil moisture estimated from GLDAS NOAH [Beaudoing and Rodell, 2020; Rodell et al., 2004] and CLSM [B. Li et al., 2019; B. Li et al., 2020] land surface models can be accesses at https://disc.gsfc.nasa.gov/datasets/GLDAS_NOAH025_M_2.1/summary and https://disc.gsfc.nasa.gov/datasets/GLDAS_CLSM025_DA1_D_2.2/summary, respectively. Precipitation estimated from the IMERG product (Huffman et al., 2019) can be accessed at https://disc.gsfc.nasa.gov/datasets/GPM_3IMERGDF_06/summary. Runoff estimation results of this study (Li & Long, 2023) are available at https://doi.org/10.5281/zenodo.7505876.

Acknowledgments
This study was financially supported by the Second Tibetan Plateau Scientific Expedition and Research (STEP) program (2019QZKK0105), the National Natural Science Foundation of China (92047301 and 92047203), and UK Research and Innovation (MR/V022008/1). Reviewers and editors' comments are highly appreciated.

References

Akbar, R., Gianotti, D. J. S., McColl, K. A., Haghighi, E., Salvucci, G. D., & Entekhabi, D. (2018). Estimation of landscape soil water losses from satellite observations of soil moisture. *Journal of Hydrometeorology*, *19*(5), 871–889. https://doi.org/10.1175/jhm-d-17-0200.1

Akbar, R., Gianotti, D. J. S., Salvucci, G. D., & Entekhabi, D. (2019). Mapped hydroclimatology of evapotranspiration and drainage runoff using SMAP brightness temperature observation and precipitation information. *Water Resources Research*, *55*(4), 3391–3413. https://doi.org/10.1029/2018wr024459

Balsamo, G., Viterbo, P., Beljaars, A., van den Hurk, B., Hirschi, M., Betts, A. K., & Scipal, K. (2009). A revised hydrology for the ECMWF model: Verification from field site to terrestrial water storage and impact in the integrated forecast system. *Journal of Hydrometeorology*, *10*(3), 623–643. https://doi.org/10.1175/2008jhm1068.1

Beaudoing, H., & Rodell, M., & NASA/GSFC/HSL. (2020). GLDAS Noah land surface model L4 monthly 0.25 x 0.25 degree V2.1 [Dataset]. Greenbelt, Maryland, USA, Goddard Earth Sciences Data and Information Services Center (GES DISC). Accessed on 30 Apr 2022. https://doi.org/10.5067/SXAVCZFAQLNO

Beck, H. E., van Dijk, A. I. J. M., de Roo, A., Dutra, E., Fink, G., Orth, R., & Schellekens, J. (2017). Global evaluation of runoff from 10 state-of-the-art hydrological models. *Hydrology and Earth System Sciences*, *21*(6), 2881–2903. https://doi.org/10.5194/hess-21-2881-2017

Berghuijs, W. R., Woods, R. A., & Hrachowitz, M. (2014). A precipitation shift from snow towards rain leads to a decrease in streamflow. *Nature Climate Change*, *4*(7), 583–586. https://doi.org/10.1038/nclimate2246

Berthier, E., Brun, F., Dussaillant, I., Farinotti, D., Girod, L., Hugonnet, R., et al. (2021). Accelerated global glacier mass loss in the early twenty-first century [Dataset]. Theia. https://doi.org/10.6096/13

Biemans, H., Siderius, C., Lutz, A. F., Nepal, S., Ahmad, B., Hassan, T., et al. (2019). Importance of snow and glacier meltwater for agriculture on the Indo-Gangetic Plain. *Nature Sustainability*, *2*(7), 594–601. https://doi.org/10.1038/s41893-019-0305-3

Brocca, L., Ciabatta, L., Moramarco, T., Ponziani, F., Berni, N., & Wagner, W. (2016). Use of satellite soil moisture products for the operational mitigation of landslides risk in central Italy (pp. 231–247).

Brocca, L., Massari, C., Ciabatta, L., Moramarco, T., Penna, D., Zuecco, G., et al. (2015). Rainfall estimation from in situ soil moisture observations at several sites in Europe: An evaluation of the SM2RAIN algorithm. *Journal of Hydrology and Hydromechanics*, *63*(3), 201–209. https://doi.org/10.1515/johh-2015-0016

Brocca, L., Moramarco, T., Melone, F., & Wagner, W. (2013). A new method for rainfall estimation through soil moisture observations. *Geophysical Research Letters*, *40*(5), 853–858. https://doi.org/10.1002/grl.50173

Brun, F., Berthier, E., Wagnon, P., Kaab, A., & Treichler, D. (2017). A spatially resolved estimate of High Mountain Asia glacier mass balances from 2000 to 2016. *Nature Geoscience*, *10*(9), 668–673. https://doi.org/10.1038/ngeo2999

Chen, X., Long, D., Hong, Y., Zeng, C., & Yan, D. (2017). Improved modeling of snow and glacier melting by a progressive two-stage calibration strategy with GRACE and multisource data: How snow and glacier meltwater contributes to the runoff of the Upper Brahmaputra River basin? *Water Resources Research*, *53*(3), 2431–2466. https://doi.org/10.1002/2016wr019656

Cheng, M., Zhong, L., Ma, Y., Zou, M., Ge, N., Wang, X., & Hu, Y. (2019). A study on the assessment of multi-source satellite soil moisture products and reanalysis Data for the Tibetan plateau. *Remote Sensing*, *11*(10), 1196. https://doi.org/10.3390/rs11101196

Ciabatta, L., Massari, C., Brocca, L., Gruber, A., Reimer, C., Hahn, S., et al. (2018). SM2RAIN-CCI: A new global long-term rainfall data set derived from ESA CCI soil moisture. *Earth System Science Data*, *10*(1), 267–280. https://doi.org/10.5194/essd-10-267-2018

filippucci, P., Tarpanelli, A., Massari, C., Serafini, A., Strati, V., Alberi, M., et al. (2020). Soil moisture as a potential variable for tracking and quantifying irrigation: A case study with proximal gamma-ray spectroscopy data. *Advances in Water Resources*, *136*, 103502. https://doi.org/10.1016/j.advwatres.2019.103502

Fischer, G., Nachtergaele, F., Prieler, S., van Velthuizen, H. T., Verelst, L., & Wiberg, D. (2008). Global agro-ecological zones assessment for agriculture (GAEZ 2008) [Dataset]. IIASA, Laxenburg, Austria and FAO. Accessed on 15 Jan 2022. Retrieved from https://www.fao.org/soils-portal/data-hub/soil-maps-and-databases/harmonized-world-soil-database-v12/en/

Georgakakos, K., & Baumer, O. W. (1996). Measurement and utilization of on-site soil moisture data. *Journal of Hydrology*, *184*(1–2), 131–152. https://doi.org/10.1016/0022-1694(95)02971-0

Ghajarnia, N., Kalantari, Z., Orth, R., & Destouni, G. (2020). Close co-variation between soil moisture and runoff emerging from multi-catchment data across Europe. *Scientific Reports*, *10*(1), 4817. https://doi.org/10.1038/s41598-020-61621-y

Gou, J., Miao, C., Samaniego, L., Xiao, M., Wu, J., & Guo, X. (2021). CNRD v1.0: A high-quality natural runoff dataset for hydrological and climate studies in China. *Bulletin of the American Meteorological Society*, *102*(5), E929–E947. https://doi.org/10.1175/bams-d-20-0094.1

Gupta, H. V., Kling, H., Yilmaz, K. K., & Martinez, G. F. (2009). Decomposition of the mean squared error and NSE performance criteria: Implications for improving hydrological modelling. *Journal of Hydrology*, *377*(1–2), 80–91. https://doi.org/10.1016/j.jhydrol.2009.08.003

Hall, D. K., & Riggs, G. A. (2007). Accuracy assessment of the MODIS snow products. *Hydrological Processes*, *21*(12), 1534–1547. https://doi.org/10.1002/hyp.6715

Han, P., Long, D., Han, Z., Du, M., Dai, L., & Hao, X. (2019). Improved understanding of snowmelt runoff from the headwaters of China's Yangtze River using remotely sensed snow products and hydrological modeling. *Remote Sensing of Environment*, *224*, 44–59. https://doi.org/10.1016/j.rse.2019.01.041

Han, Z., Long, D., Fang, Y., Hou, A., & Hong, Y. (2019). Impacts of climate change and human activities on the flow regime of the dammed Lancang River in Southwest China. *Journal of Hydrology*, *570*, 96–105. https://doi.org/10.1016/j.jhydrol.2018.12.048

Han, Z., Long, D., Han, P., Huang, Q., Du, M., & Hou, A. (2021). An improved modeling of precipitation phase and snow in the Lancang River Basin in Southwest China. *Science China Technological Sciences*, *64*(7), 1513–1527. https://doi.org/10.1007/s11431-020-1788-4

Han, Z., Long, D., Huang, Q., Li, X., Zhao, F., & Wang, J. (2020). Improving reservoir outflow estimation for ungauged basins using satellite observations and a hydrological model. *Water Resources Research*, *56*(9), e2020WR027590. https://doi.org/10.1029/2020wr027590

Hong, Z., Han, Z., Li, X., Long, D., Tang, G., & Wang, J. (2021). Generation of an improved precipitation Dataset from multisource information over the Tibetan plateau. *Journal of Hydrometeorology*, *22*(5), 1275–1295. https://doi.org/10.1175/jhm-d-20-0252.1

Huang, Q., Long, D., Du, M., Han, Z., & Han, P. (2020). Daily continuous river discharge estimation for ungauged basins using a hydrologic model calibrated by satellite altimetry: Implications for the SWOT mission. *Water Resources Research*, *56*(7), e2020WR027309. https://doi.org/10.1029/2020wr027309

Huang, Q., Long, D., Han, Z., & Han, P. (2022). High-resolution satellite images combined with hydrological modeling derive river discharge for headwaters: A step toward discharge estimation in ungauged basins. *Remote Sensing of Environment*, *277*, 113030. https://doi.org/10.1016/j.rse.2022.113030

Huffman, G. J., Stocker, E. F., Bolvin, D. T., Nelkin, E. J., & Tan, J. (2019). GPM IMERG final precipitation L3 1 day 0.1 degree x 0.1 degree V06. [Dataset]. In A. Savtchenko, & M. D. Greenbelt (Eds.), *Goddard earth Sciences Data and Information Services Center (GES DISC)*. Accessed on 20 Feb 2022. https://doi.org/10.5067/GPM/IMERGDF/DAY/06

Huggins, X., Gleeson, T., Kummu, M., Zipper, S. C., Wada, Y., Troy, T. J., & Famiglietti, J. S. (2022). Hotspots for social and ecological impacts from freshwater stress and storage loss. *Nature Communications*, *13*(1), 439. https://doi.org/10.1038/s41467-022-28029-w

Hugonnet, R., McNabb, R., Berthier, E., Menounos, B., Nuth, C., Girod, L., et al. (2021). Accelerated global glacier mass loss in the early twenty-first century. *Nature*, *592*(7856), 726–731. https://doi.org/10.1038/s41586-021-03436-z

Huss, M. (2013). Density assumptions for converting geodetic glacier volume change to mass change. *The Cryosphere*, *7*(3), 877–887. https://doi.org/10.5194/tc-7-877-2013

Immerzeel, W. W., Lutz, A. F., Andrade, M., Bahl, A., Biemans, H., Bolch, T., et al. (2020). Importance and vulnerability of the world's water towers. *Nature*, *577*(7790), 364–369. https://doi.org/10.1038/s41586-019-1822-y

Immerzeel, W. W., Lutz, A. F., Andrade, M., Bahl, A., Biemans, H., Bolch, T., et al. (2019). Supplementary data to: Importance and vulnerability of the world's water towers (1.0). [Dataset]. Zenodo. https://doi.org/10.5281/zenodo.3521933

Immerzeel, W. W., Pellicciotti, F., & Bierkens, M. F. P. (2013). Rising river flows throughout the twenty-first century in two Himalayan glacierized watersheds. *Nature Geoscience*, *6*(9), 742–745. https://doi.org/10.1038/ngeo1896

Immerzeel, W. W., van Beek, L. P. H., & Bierkens, M. F. P. (2010). Climate change will affect the Asian water towers. *Science*, *328*(5984), 1382–1385. https://doi.org/10.1126/science.1183188

Immerzeel, W. W., Wanders, N., Lutz, A. F., Shea, J. M., & Bierkens, M. F. P. (2015). Reconciling high-altitude precipitation in the upper Indus basin with glacier mass balances and runoff. *Hydrology and Earth System Sciences*, *19*(11), 4673–4687. https://doi.org/10.5194/hess-19-4673-2015

Jahlvand, E., Tajrishy, M., Brocca, L., Massari, C., Hashemi, S. G. Z., & Ciabatta, L. (2018). Estimating the drainage rate from surface soil moisture drydowns: Application of DfD model to in situ soil moisture data. *Journal of Hydrology*, *565*, 489–501. https://doi.org/10.1016/j.jhydrol.2018.08.035

Jiang, B. (2015). Head/tail breaks for visualization of city structure and dynamics. *Cities*, *43*, 69–77. https://doi.org/10.1016/j.cities.2014.11.013

Jiang, B., Liu, X., & Jia, T. (2013). Scaling of geographic space as a universal rule for map generalization. *Annals of the Association of American Geographers*, *103*(4), 844–855. https://doi.org/10.1080/00045608.2013.765773

Jin, H., He, R., Cheng, G., Wu, Q., Wang, S., Lue, L., & Chang, X. (2009). Changes in frozen ground in the source area of the Yellow river on the Qinghai-Tibet plateau, China, and their eco-environmental impacts. *Environmental Research Letters*, *4*(4), 045206. https://doi.org/10.1088/1748-9326/4/4/045206

Kling, H., Fuchs, M., & Paulin, M. (2012). Runoff conditions in the upper Danube basin under an ensemble of climate change scenarios. *Journal of Hydrology*, *424*, 264–277. https://doi.org/10.1016/j.jhydrol.2012.01.011

Koster, R. D., Crow, W. T., Reichle, R. H., & Mahanama, S. P. (2018). Estimating basin-scale water budgets with SMAP soil moisture data. *Water Resources Research*, *54*(7), 4228–4244. https://doi.org/10.1029/2018wr022669

Kraaijenbrink, P. D. A., Stigter, E. E., Yao, T., & Immerzeel, W. W. (2021). Climate change decisive for Asia's snow meltwater supply. *Nature Climate Change*, *11*(7), 591–597. https://doi.org/10.1038/s41558-021-01074-x

Kratzert, F., Klotz, D., Shalev, G., Klambauer, G., Hochreiter, S., & Nearing, G. (2019). Towards learning universal, regional, and local hydrological behaviors via machine learning applied to large-sample datasets. *Hydrology and Earth System Sciences*, *23*(12), 5089–5110. https://doi.org/10.5194/hess-23-5089-2019

Li, B., Beaudoing, H., & Rodell, M., & NASA/GSFC/HSL. (2020). GLDAS catchment land surface model L4 daily 0.25 x 0.25 degree GRACE-DA1 V2.2. [Dataset]. Greenbelt, Maryland, USA, Goddard Earth Sciences Data and Information Services Center (GES DISC). Accessed on 20 Mar 2022. https://doi.org/10.5067/TXBMLX370XX8

Li, B., Rodell, M., Kumar, S., Beaudoing, H. K., Getirana, A., Zaitchik, B. F., et al. (2019). Global GRACE data assimilation for groundwater and drought monitoring: Advances and challenges. *Water Resources Research*, *55*(9), 7564–7586. https://doi.org/10.1029/2018wr024618

Li, X., & Long, D. (2020). An improvement in accuracy and spatiotemporal continuity of the MODIS precipitable water vapor product based on a data fusion approach. *Remote Sensing of Environment*, *248*, 111966. https://doi.org/10.1016/j.rse.2020.111966

Li, X., & Long, D. (2023). Supplementary data to: Soil Moisture to Runoff (SM2R) A data-driven model for runoff estimation across poorly gauged Asian water towers based on soil moisture dynamics [Dataset]. Zenodo. https://doi.org/10.5281/zenodo.7505876

Li, X., Long, D., Han, Z., Scanlon, B. R., Sun, Z., Han, P., & Hou, A. (2019). Evapotranspiration estimation for Tibetan Plateau headwaters using conjoint terrestrial and atmospheric water balances and multisource remote sensing. *Water Resources Research*, *55*(11), 8608–8630. https://doi.org/10.1029/2019wr025196

Li, X., Long, D., Huang, Q., & Zhao, F. (2022). The state and fate of lake ice thickness in the Northern Hemisphere. *Science Bulletin*, *67*(5), 537–546. https://doi.org/10.1016/j.scib.2021.10.015

Li, X., Long, D., Scanlon, B. R., Mann, M. E., Li, X., Tian, F., et al. (2022). Climate change threatens terrestrial water storage over the Tibetan Plateau. *Nature Climate Change*, *12*(9), 801–807. https://doi.org/10.1038/s41558-022-01443-0

Liu, W., Sun, F., Li, Y., Zhang, G., Sang, Y.-F., Lim, W. H., et al. (2018). Investigating water budget dynamics in 18 river basins across the Tibetan Plateau through multiple datasets. *Hydrology and Earth System Sciences*, *22*(1), 351–371. https://doi.org/10.5194/hess-22-351-2018

Liu, W., Wang, L., Chen, D., Tu, K., Ruan, C., & Hu, Z. (2016). Large-scale circulation classification and its links to observed precipitation in the eastern and central Tibetan Plateau. *Climate Dynamics*, *46*(11–12), 3481–3497. https://doi.org/10.1007/s00382-015-2782-z

Liu, W., Wang, L., Sun, F., Li, Z., Wang, H., Liu, J., et al. (2018). Snow hydrology in the upper Yellow river basin under climate change: A land surface modeling perspective. *Journal of Geophysical Research-Atmospheres*, *123*(22), 12676–12691. https://doi.org/10.1029/2018jd028984

Long, D., Li, X., Scanlon, B. R., Mann, M. E., Li, X., Tian, F., et al. (2022). Water loss over the Tibetan Plateau endangers water supply security for Asian populations. *Nature Climate Change*, *12*(9), 801–807. https://doi.org/10.1038/s41558-022-01443-0

Lutz, A. F., Immerzeel, W. W., Shrestha, A. B., & Bierkens, M. F. P. (2014). Consistent increase in High Asia's runoff due to increasing glacier melt and precipitation. *Nature Climate Change*, *4*(7), 587–592. https://doi.org/10.1038/nclimate2237

Lutz, A. F., Immerzeel, W. W., Siderius, C., Wijngaard, R. R., Nepal, S., Shrestha, A. B., et al. (2022). South Asian agriculture increasingly dependent on meltwater and groundwater. *Nature Climate Change*, *12*(6), 566–573. https://doi.org/10.1038/s41558-022-01355-z

Mastrotheodoros, T., Pappas, C., Molnar, P., Burlando, P., Manoli, G., Parajka, J., et al. (2020). More green and less blue water in the Alps during warmer summers. *Nature Climate Change*, *10*(2), 155–161. https://doi.org/10.1038/s41558-019-0676-5

Muñoz Sabater, J. (2019). ERA5-Land monthly averaged data from 1981 to present [Dataset]. Copernicus Climate Change Service (C3S) Climate Data Store (CDS). Accessed on 1 Oct 2021. https://doi.org/10.24381/cds.68d2bb30

Munoz-Sabater, J., Dutra, E., Agusti-Panareda, A., Albergel, C., Arduini, G., Balsamo, G., et al. (2021). ERA5-Land: A state-of-the-art global reanalysis dataset for land applications. *Earth System Science Data*, *13*(9), 4349–4383. https://doi.org/10.5194/essd-13-4349-2021

Nash, J. E., & Sutcliffe, J. V. (1970). River flow forecasting through conceptual models part I-A discussion of principles. *Journal of Hydrology*, *10*(3), 282–290. https://doi.org/10.1016/0022-1694(70)90255-6

RGI Consortium. (2017). Randolph glacier inventory - A Dataset of global glacier outlines, Version 6. [Dataset]. National Snow and Ice Data Center. Accessed on 17 Nov 2021. https://doi.org/10.7265/4m1f-gd79

Rodell, M., Houser, P. R., Jambor, U., Gottschalck, J., Mitchell, K., Meng, C. J., et al. (2004). The global land data assimilation system. *Bulletin of the American Meteorological Society*, *85*(3), 381–394. https://doi.org/10.1175/bams-85-3-381

Santhi, C., Arnold, J. G., Williams, J. R., Dugas, W. A., Srinivasan, R., & Hauck, L. M. (2001). Validation of the swat model on a large river basin with point and nonpoint sources. *Journal of the American Water Resources Association*, *37*(5), 1169–1188. https://doi.org/10.1111/j.1752-1688.2001.tb03630.x

Satoh, Y., Yoshimura, K., Pokhrel, Y., Kim, H., Shiogama, H., Yokohata, T., et al. (2022). The timing of unprecedented hydrological drought under climate change. *Nature Communications*, *13*(1), 3287. https://doi.org/10.1038/s41467-022-30729-2

Shangguan, W., Dai, Y., Duan, Q., Liu, B., & Yuan, H. (2014). A global soil data set for Earth system modeling. *Journal of Advances in Modeling Earth Systems*, *6*(1), 249–263. https://doi.org/10.1002/2013ms000293

Shi, R., Yang, H., & Yang, D. (2020). Spatiotemporal variations in frozen ground and their impacts on hydrological components in the source region of the Yangtze River. *Journal of Hydrology*, *590*, 125237. https://doi.org/10.1016/j.jhydrol.2020.125237

Sivapalan, M., Takeuchi, K., Franks, S. W., Gupta, V. K., Karambiri, H., Lakshmi, V., et al. (2003). IAHS decade on Predictions in Ungauged Basins (PUB), 2003-2012: Shaping an exciting future for the hydrological sciences. *Hydrological Sciences Journal-Journal Des Sciences Hydrologiques*, *48*(6), 857–880. https://doi.org/10.1623/hysj.48.6.857.51421

Su, F., Zhang, L., Ou, T., Chen, D., Yao, T., Tong, K., & Qi, Y. (2016). Hydrological response to future climate changes for the major upstream river basins in the Tibetan Plateau. *Global and Planetary Change*, *136*, 82–95. https://doi.org/10.1016/j.gloplacha.2015.10.012

Vorosmarty, C. J., Green, P., Salisbury, J., & Lammers, R. B. (2000). Global water resources: Vulnerability from climate change and population growth. *Science*, *289*(5477), 284–288. https://doi.org/10.1126/science.289.5477.284

Wang, J., Hong, Y., Li, L., Gourley, J. J., Khan, S. I., Yilmaz, K. K., et al. (2011). The coupled routing and excess storage (CREST) distributed hydrological model. *Hydrological Sciences Journal-Journal Des Sciences Hydrologiques*, *56*(1), 84–98. https://doi.org/10.1080/02626667.2010.543087

Wang, T., Yang, D., Qin, Y., Wang, Y., Chen, Y., Gao, B., & Yang, H. (2018). Historical and future changes of frozen ground in the upper Yellow River Basin. *Global and Planetary Change*, *162*, 199–211. https://doi.org/10.1016/j.gloplacha.2018.01.009

Wu, Y., Long, D., Lall, U., Scanlon, B. R., Tian, F., Fu, X., et al. (2022). Reconstructed eight-century streamflow in the Tibetan Plateau reveals contrasting regional variability and strong nonstationarity. *Nature Communications*, *13*(1), 6416. https://doi.org/10.1038/s41467-022-34221-9

Xing, Z., Fan, L., Zhao, L., De Lannoy, G., Frappart, F., Peng, J., et al. (2021). A first assessment of satellite and reanalysis estimates of surface and root-zone soil moisture over the permafrost region of Qinghai-Tibet Plateau. *Remote Sensing of Environment*, *265*, 112666. https://doi.org/10.1016/j.rse.2021.112666

Yang, J., Ding, Y., Chen, R., & Shen, Y. (2004). Permafrost change and its effect on eco-environment in the source regions of the Yangtze and Yellow rivers. *Journal of Mountain Science*, *22*(3), 278–285.

Yao, T. (2022). *The imbalance of the Asian water tower*. Nature Reviews Earth & Environment.

Yao, Y., & Zhang, B. (2013). MODIS-based estimation of air temperature of the Tibetan Plateau. *Journal of Geographical Sciences*, *23*(4), 627–640. https://doi.org/10.1007/s11442-013-1033-7

Yue, S., Wang, B., Yang, K., Xie, Z., Lu, H., & He, J. (2021). Mechanisms of the decadal variability of monsoon rainfall in the southern Tibetan Plateau. *Environmental Research Letters*, *16*(1), 014011. https://doi.org/10.1088/1748-9326/abcb36

Zhao, F., Long, D., Li, X., Huang, Q., & Han, P. (2022). Rapid glacier mass loss in the Southeastern Tibetan Plateau since the year 2000 from satellite observations. *Remote Sensing of Environment*, *270*, 112853. https://doi.org/10.1016/j.rse.2021.112853

Zhao, Q., Ding, Y., Wang, J., Gao, H., Zhang, S., Zhao, C., et al. (2019). Projecting climate change impacts on hydrological processes on the Tibetan Plateau with model calibration against the glacier inventory data and observed streamflow. *Journal of Hydrology*, *573*, 60–81. https://doi.org/10.1016/j.jhydrol.2019.03.043